ACS NANO

www.acsnano.org

PERSPECTIVE

Bridging the *In Vitro* to *In Vivo* gap: Using the Chick Embryo Model to Accelerate Nanoparticle Validation and Qualification for *In Vivo* studies

Kimberly S. Butler, C. Jeffrey Brinker, and Hon Sing Leong*

Cite This: *ACS Nano* 2022, 16, 19626–19650

Read Online

ACCESS | Metrics & More | Article Recommendations | Supporting Information

ABSTRACT: We postulate that nanoparticles (NPs) for use in therapeutic applications have largely not realized their clinical potential due to an overall inability to use *in vitro* results to predict NP performance *in vivo*. The avian embryo and associated chorioallantoic membrane (CAM) has emerged as an *in vivo* preclinical model that bridges the gap between *in vitro* and *in vivo*, enabling rapid screening of NP behavior under physiologically relevant conditions and providing a rapid, accessible, economical, and more ethical means of qualifying nanoparticles for *in vivo* use. The CAM is highly vascularized and mimics the diverging/converging vasculature of the liver, spleen, and lungs that serve as nanoparticle traps. Intravital imaging of fluorescently labeled NPs injected into the CAM vasculature enables immediate assessment and quantification of nano-bio interactions at the individual NP scale in any tissue of interest that is perfused with a microvasculature. In this review, we highlight how utilization of the avian embryo and its CAM as a preclinical model can be used to understand NP stability in blood and tissues, extravasation, biocompatibility, and NP distribution over time, thereby serving to identify a subset of NPs with the requisite stability and performance to introduce into rodent models and enabling the development of structure–property relationships and NP optimization without the sacrifice of large populations of mice or other rodents. We then review how the chicken embryo and CAM model systems have been used to accelerate the development of NP delivery and imaging agents by allowing direct visualization of targeted (active) and nontargeted (passive) NP binding, internalization, and cargo delivery to individual cells (of relevance for the treatment of leukemia and metastatic cancer) and cellular ensembles (e.g., cancer xenografts of interest for treatment or imaging of cancer tumors). We conclude by showcasing emerging techniques for the utilization of the CAM in future nano-bio studies.

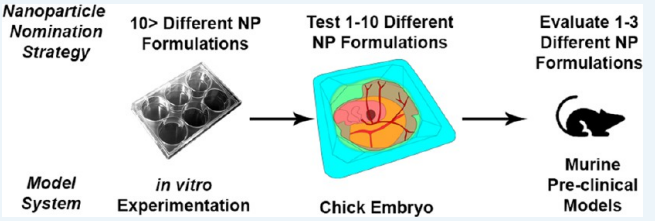

KEYWORDS: *chick embryo, nanoparticle development, chorioallantoic membrane, nanoparticle bioavailability, drug development, intravital imaging, structure–function analysis*

INTRODUCTION: RATIONALE FOR AN INTERMEDIATE PRECLINICAL MODEL FOR BIO-NANO RESEARCH

In 2018, MIRIBEL (minimum information reporting in bio-nano experimental literature) standards were established to stipulate how nanoparticles (NPs) intended for biomedical applications are to be characterized and how their *in vitro* interactions within any biological system are to be described and evaluated in the literature.[1] MIRIBEL defined a checklist of specific components to be reported, divided into three categories: material characterization, biological characterization, and details of experimental protocols with the intention of improving reproducibility, increasing quantitative comparisons of bio-nano materials, and facilitating meta-analyses and *in silico* modeling. In response to the publication of MIRIBEL in *Nature Nanotechnology*, the bio-nano research community was invited to provide suggestions to further these guidelines.[2] We advocated for an *ex ovo* model system to "bridge the gap" between *in vitro* assessments of NPs stipulated by MIRIBEL and *in vivo* rodent models. Our rationale was that, in spite of many successful *in vitro* studies, nanoparticle delivery systems have not achieved their anticipated potential *in vivo* or in the

Received: April 23, 2022
Accepted: October 17, 2022
Published: December 1, 2022

https://doi.org/10.1021/acsnano.2c03990
ACS Nano 2022, 16, 19626–19650

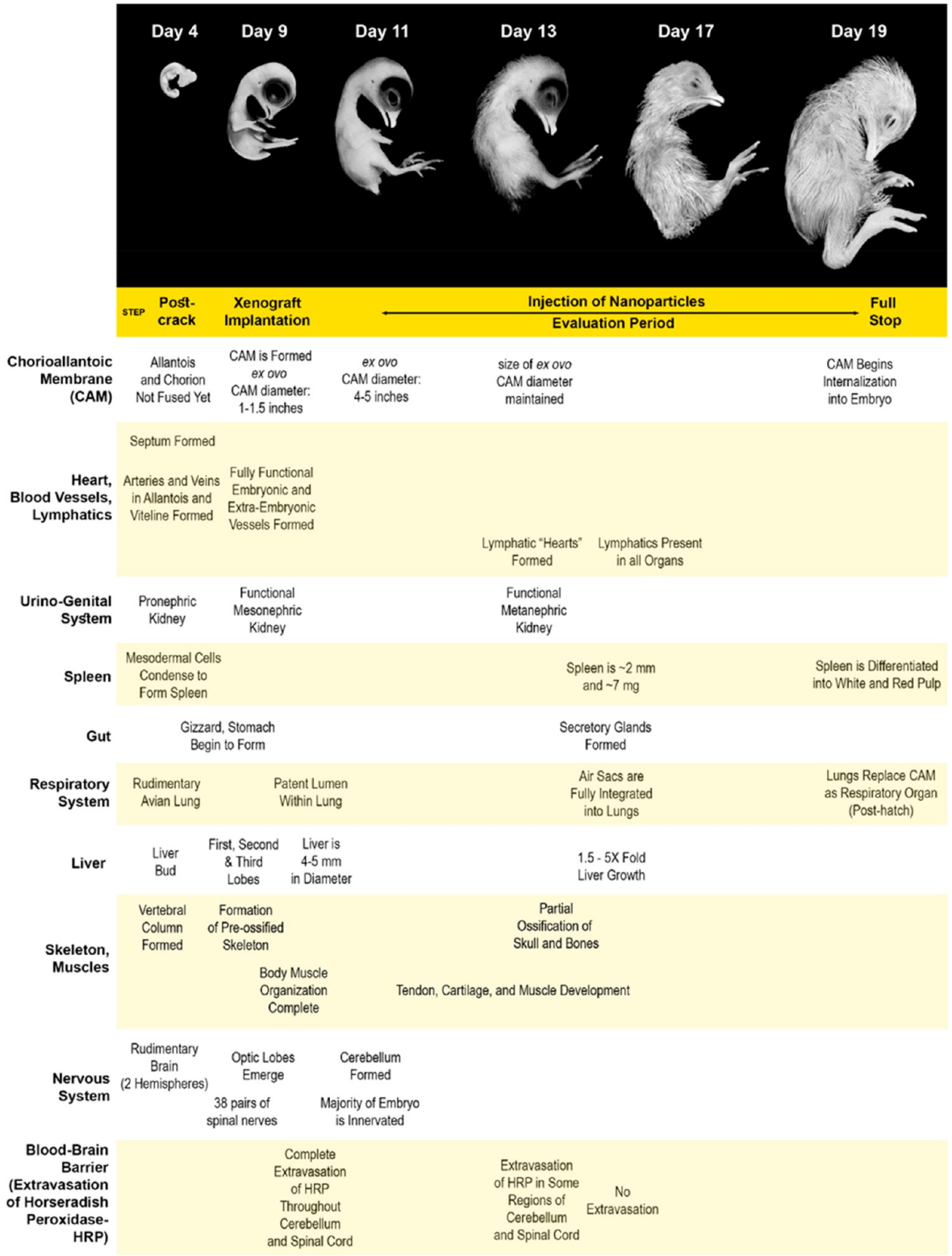

Figure 1. Developmental timeframe of the chick embryo (CE). Highlighted stages of CE development relevant to their usage in biomedical research and NP formulation assessment. This is not an exhaustive list and contains biological events relevant to possible experimental procedures.[24−28] Images are adapted with permission from ref 24. Copyright 2014 Academic Press.

clinic. This deficiency has been documented in a recent meta-analysis of 117 studies of nanoparticle delivery to solid tumors conducted from 2005 to 2015, where it was concluded that a median of 0.7% of the intravenously injected dose reached the tumor and that this value had not improved over the course of 10 years.[3] Lack of NP uptake into tumors via passive or active targeting is the greatest current barrier in NP development.[3] Reduced NP uptake is a consequence of processes such as NP aggregation, rapid uptake by the mononuclear phagocyte system (MPS), nonspecific binding, and renal clearance. These

https://doi.org/10.1021/acsnano.2c03990
ACS Nano 2022, 16, 19626−19650

clearance mechanisms are not present in *in vitro* investigations. Therefore, most studies to date have been evaluated almost exclusively in costly, time-consuming, and in some cases, unethical rodent models. Here it is noteworthy that more than 100 million rodents are believed to be used annually for experiments in the U.S. alone.[4] Engineering NP physicochemical parameters to overcome these instability mechanisms requires an alternative preclinical model amenable to visualization of NP interactions *in vivo* that is accessible, affordable, and fast.[5] We proposed utilization of the chorioallantoic membrane (CAM) of the chick/avian embryo as a rapid, physiologically relevant, economical, and more ethical preclinical model to evaluate nanoparticle stability and qualify nanoparticles for *in vivo* use in mammals.[2,6] Through optical labeling of NPs, target cells, off-target cells, and tissues, intravital imaging in the CAM provides the researcher immediate visualization of NP pharmacokinetics and the ability to successively overcome multiple physiological barriers needed to achieve therapeutic efficacy or serve as imaging agents: namely, (1) unwanted interactions with plasma proteins and blood cells, (2) extravasation past the vascular barrier, and (3) unwanted interstitial fluid interactions with NPs prior to uptake into target cells. Furthermore, by coinjection of labeled, target cells (healthy/disease phenotype) or xenografting of tumors to the CAM, NP binding/targeting, internalization, and drug release under physiologically relevant conditions at the single-NP scale can be directly observed. Understanding pharmacodynamics at the microscopic level of the NP is critical in the determination of therapeutic efficacy, which depends on quantification of the percent administered dose or number of NPs that arrive at the target cell/tumor and the ensuing events of (1) NP uptake by various cells of the tumor and its microenvironment (i.e., endothelial cells, tissue macrophages, fibroblasts, fibrotic areas, etc.), (2) extent of active (triggered) or passive release of the cargo by desorption and/or NP degradation, and (3) successful NP trafficking to the appropriate intracellular space (i.e., cytosol or nucleus). In all cases it is important to apply the correct metric with respect to the anticipated antitumor response (i.e., tumor volume changes upon treatment with cytotoxic payloads, tumor vascularity with antiangiogenic therapies, and tumor metabolism via fluorodeoxyglucose-positron emission tomography (FDG-PET)).

Hence, we describe in detail the chorioallantoic membrane (CAM) of the avian embryo model, which allows a rapid assessment of the key determinants of NP performance in an economical, accessible *tissue culture* model. These models facilitate rapid iterations on NP properties and can thereby qualify candidate NPs for administration to rodents and higher-order mammalian models.

CHARACTERISTICS OF THE AVIAN EMBRYO AND CHORIOALLANTOIC MEMBRANE MODELS AND THEIR USE IN BIOMEDICAL RESEARCH

Preclinical studies typically include both *in vitro* and *in vivo* animal models. Animal models provide critical information such as disease progression, therapeutic efficacy, off-target events, and toxicity that is difficult to achieve with *in vitro* models. While animal models provide critical information, there is a drive to reduce animal use following the 3Rs concept of reduction, replacement, and refinement.[7] As a result, a wide number of tools have been developed to enable the evaluation of complex interactions without the use of animal models, including three-dimensional (3D) cell culture models such as multicellular tumor spheroids and 3D scaffold cultures.[8−11] 3D culture systems can provide insight into cell−cell and cell−matrix interactions and the effects of physiochemical gradients. However, most of these systems do not mimic blood flow or complex stroma. To address these limitations with the initial 3D systems, microfluidics has been added to 3D culture systems and complex organ-on-a-chip systems have been developed.[12−15] These complex systems are advancing rapidly and continually developing more systems such as a microengineered human blood−brain barrier platform and a geometry-tunable artery system.[16,17] While these systems are continually developing and can provide critical insight into the behavior of nanomaterials,[18−22] they are often limited by the absence of features such as blood/flow perfusion, vascular infiltration, complexity of fabrication, and the inability in some systems to readily retrieve the biological sample for further analysis. Furthermore, these systems cannot readily mimic different administration routes and provide limited information on off-target effects, pharmacokinetics, toxicology, and in the case of cancer therapeutics, changes in metastatic potential. In these areas, the avian/chick embryo and its chorioallantoic membrane can provide critical insight while still meeting the goal of the 3Rs for animal use.

There are numerous benefits to the use of the embryonic avian as a model system to bridge the *in vitro* to *in vivo* gap. Most commonly used is the*Gallus gallus* avian organism, or domestic chicken, whose embryo when used in scientific contexts is colloquially termed the chick embryo (CE). The developmental timeline and body plan of the chick embryo is well-characterized[23,24] and graphically described in Figure 1. CEs are easy to manipulate and amenable to a variety of imaging techniques, allowing direct visualization of stability, biocompatibility, circulation, delivery, degradation, and therapeutic efficacy—key predictors of *in vivo* performance in rodents and higher-order mammals. Furthermore, the CE model is inexpensive, exhibits rapid growth compared to mammalian model systems, can be handled and grown in most laboratories rather than in animal facilities, and (up until 21 days) is viewed to be a 3D tissue culture model for the purposes of garnering IUCAC (Institutional Animal Care and Use Committee) approval. Together, these advantages make the CE easier to handle, more rapid for analysis, and overall less costly. Furthermore, the CE has a chorioallantoic membrane (CAM) that is an easily accessible, highly vascular tissue that is amenable to tumor xenografts (patient primary cells or cell lines) and allows direct vascular injection and intravital imaging. Due to these combined features, the qualification/certification of nanoparticles (and more broadly medicines) via testing *in vivo* within the CAM is predicted to reduce the use and increase the success of rodent model studies.

A short discussion of immune mechanisms is needed, since there are immunological reactions to foreign invaders such as NPs and tumor xenografts in the CAM of CEs. There are innate immune mechanisms and adaptive immune mechanisms. Innate immunity within the CAM consists of three main mechanisms: the bactericidal properties of various proteins in the egg white[29] and the abundance of lung surfactant that lines the CAM exterior and traps foreign bodies before they penetrate further into any cells in the CAM and macrophage cells.[30] However, the first two innate mechanisms do not influence NPs or tumor xenografts due to their external

https://doi.org/10.1021/acsnano.2c03990
ACS Nano 2022, 16, 19626−19650

Figure 2. Chicken embryo and chorioallantoic membrane (CAM) models for biomedical research. (A) *In ovo* chicken embryo model showing an early stage post fertilization. Reprinted with permission from ref 31. Copyright 2020 Elsevier. (B) *Ex ovo* chicken embryo model with visible CAM overlaying the embryo. Adapted with permission from ref 6. Copyright 2010 Nature Publishing Group. (C) The CAM vascular network visualized by assembly of single photographic frames. Open arrows indicate major venous vessels, and filled arrows indicate major arterial vessels.[44] (D–F) Scanning electron microscope (SEM) images of the CAM vessel network. The CAM is inverted in the SEM preparations to allow clear visualization of the capillary plexus (*) both fed and drained from below by large vessels. Arrowheads signify feeding arterioles into the CAM or departing venules from the CAM plexus into a larger artery or vein, respectively. Reprinted with permission from ref 44. Copyright 2016 The American Physiological Society (APS).

location away from the embryo and the ability to directly bypass these mechanisms through direct injection into the CAM vasculature. Macrophage-like cells with phagocytic activity are present within the yolk sac by days 2–4 and present in the liver as early as day 12.[30] By day 12, these cells are functionally competent and can perform chemotaxis and phagocytose material.[30] These cells can phagocytose and sequester nanoparticles and other foreign material. These interactions can provide an early indication of nanomaterials that might be rapidly cleared from circulation.

In terms of adaptive immunity, the chick embryo develops various lymphoid organs such as the thymus and the bursa of Fabricius, which are sites of lymphocyte antigen processing needed for cell-mediated and antibody-mediated lymphocyte development.[30] Although these begin to form at days 3–18, these organs do not generate enough cells to mount a response against tumor xenografts. This is seen by the initial population of cells within the bursa at days 8–14 and subsequent gene arrangements for variable regions of any IgY immunoglobulin occurring until days 15–20. Therefore, a humoral-based adaptive immune response does not robustly occur until after hatching (day 21).[30] In terms of cell-based adaptative immune responses, there are macrophage-like cells in the yolk sac that can release various cytokines such as IL-1β, IL-8, IL-12, and IL-18. However, lymphocytes (also termed granulocytes) do not begin to differentiate into their cytotoxic phenotypes until day 15. These are mostly NK cells that are not antigen-specific. Hence, the majority of lymphocyte subsets that comprise any adaptive immune response do not arise until after hatching (day 21).[30] These properties make the chick embryo an excellent host for accommodating a wide variety of mammalian cell types, including tumor cells. When they are implanted into the CAM, these xenografts are readily accessible for subsequent physical/pharmacological interventions and longitudinal imaging.

To allow direct visualization of nanoparticle behavior over time, the *in ovo* and *ex ovo* methods can both be used (Figure 2A,B). In the *in ovo* model, a window is cut into the shell of the fertilized egg and then covered to prevent dehydration or infection (Figure 2A). In the *ex ovo* model system, the embryo is removed from the shell and grown in a covered dish. Each method has advantages; the *in ovo* method increases survival and facilitates the natural calcium exchange from the shell,[31] while the *ex ovo* method allows greater access to the embryo, increasing the applicable imaging modalities.[6] Due the ability to directly observe its development and rapid developmental timeline, the CE has been invaluable historically for studies of embryo and organ development, including neural, limb, and cardiac development.[32–34] These same features make the CE a common model for studying the adverse effects of drugs, viruses, and compounds.[32] For example, the CE has been used to evaluate the teratology of thalidomide, the Zika virus, and fetal alcohol syndrome disorders.[32,35] Beyond developmental studies, the CE model facilitates rapid assessment of drugs delivered topically, vascularly, or directly into the body of the embryo or into the yolk sac and amnion.[36,37] Analyses of drug behavior include embryo mortality, egg/embryo weight, developmental alterations, serum biomarkers, biodistribution to organs, and histopathology of organs.[36–38] The CE model has also been used for studying infection and virulence of bacteria and fungus.[39–43] Infection and virulence were assessed via embryonal death, a histological assessment of organs, a reverse transcription-polymerase chain reaction (RT-PCR) for alterations in chemokines and cytokines, and an enzyme-linked immunoassay (ELISA) for antibody production.[39–41,43]

Within the CE, the chorioallantoic membrane (CAM) acts as a convenient vascular model system for research. The CAM acts as a respiratory organ for the developing embryo and is a thin, transparent, and highly vascularized membrane composed of the capillary plexus, veins, and arteries (Figure 2C–F). The

https://doi.org/10.1021/acsnano.2c03990
ACS Nano 2022, 16, 19626–19650

CAM vasculature undergoes rapid angiogenesis during development, making it a common model for vascular irritation and angiogenesis.[45,46] The vascular development of the CAM takes place during the first 11 days, facilitating experimentation on both rapidly developing vessels during the first 11 days and on mature vessels day 12 and beyond. Due to this versatility, the CAM allows a rapid review of potential antiangiogenic molecules and drug combinations through visualization of their effect on the CAM.[47−50] Recently, direct imaging has been combined with quantification of vessel length and number of junctions as a metric of vascular damage caused by pharmacological intervention.[47] While most studies observe effects on CAM vessels after a period of time, the superficial location of the CAM with respect to the embryo and its thinness allow monitoring of therapeutic effects in real time by intravital imaging.[51] Due to the importance of angiogenesis in wound healing and the accessibility of the model, the CAM has been extensively used to assess the potential of therapeutics and treatments for wound healing.[52] For example, the CAM was utilized to assess carbon monoxide releasing molecules,[53] polyherbal formulations,[54] photodynamic therapy with photosensitizers,[55,56] and photomodulation of angiogenesis for wound healing.[57]

While cancer studies are not the only use of the CAM model, the ready accessibility and ability to accommodate a wide range of both normal and tumor xenografts makes the CAM an attractive model.[58,59] It is therefore worthwhile to look at the tumor microenvironment within the CAM. The CAM is multilayered, consisting of an ectoderm at the air interface, a vascularized mesoderm, and an endoderm at the interface with the allantoic sac.[58,60] The mesoderm consists of an extracellular matrix (ECM), blood and lymphatic vessels, and fibroblasts similar to mammalian tumor stroma.[58] This combination of features allows an evaluation of the interaction of xenograft tumors with the stroma. The most well studied tumor xenograft interaction in the CAM is angiogenesis and tumor spread via blood vessels.[59] For example, Epstein−Barr virus (EBV) positive lymphoma cells have an increased ability to disrupt the stroma and invade tissue, demonstrating spread along blood vessels and lymphatics when compared to EBV-negative lymphoma cells.[61] Beyond invasion and spread, tumor-induced angiogenesis can also be monitored in the CAM. Glioma cells induced angiogenesis and infiltration of CAM vasculature into the tumor via vascular endothelial growth factor receptor-2 (VEGFR-2) and recapitulation of the molecular angiogenic switch found in human tumors.[62] Beyond cell line xenografts, patient-derived xenografts, which contain human blood vessels, can be utilized. Individual molecular markers of chicken- and human-derived blood vessels can be used to differentiate the vessels that began in the tumor tissue and those induced from the CAM.[63]

In addition to studying blood vessel interactions between xenografts and the CAM, the presence of ECM facilitates studies of stromal matrix interactions.[59] The ECM of the CAM mesoderm includes a variety of matrix proteins such as fibronectin, laminin, collagen type I, and integrin $\alpha v\beta_3$, which mimics the physiological tumor microenvironment.[60] Both cell-line- and patient-derived xenografts have demonstrated invasive behavior into the CAM, allowing studies of invasion, including comparison studies between tumor types and specific tumor features.[61−64] For example, low-grade chondrosarcomas were unable to invade while high-grade chondrosarcomas showed extensive invasion mimicking the situation in humans.[64] Beyond simple invasion observations, molecular interactions of tumor cells with the ECM can be studied in the CAM. Xenografts in the CAM have been used to understand the contributions of ECM-modifying proteins such as matrix metalloproteinases (MMPs), urokinase plasminogen activator (uPA), and uPA receptor (uPAR) in tumor invasion of the ECM.[65,66] One potential shortfall of the CAM system is that avian cells present in the stroma do not recapitulate all features of human tumor stromal cells, which has implications that vary based on tumor type. For example, pancreatic stellate cells are integral to the disease progression of pancreatic adenocarcinoma and are not present in the CAM. One method around this shortcoming is to cograft the tumor-associated cells with tumor cells either from mixing cell cultures or using patient-derived xenografts. In the case of pancreatic cancer, increased tumor growth and invasion was observed when pancreatic stellate cells were cografted with pancreatic cancer cell lines.[67] While the CAM recapitulates much of the tumor stroma, there are some differences between avian and human cells and proteins that require careful examination for each tumor type.

Overall, due to the ease of use and low cost, the CAM model is being developed for many areas of biomedical science. As described in the following sections, one of the most promising areas of CAM development is the evaluation of nanoparticles as delivery and imaging agents in oncology, where the CAM system has been developed for a broad range of cancer types,[68] including patient-derived xenografts,[69] and for studies in cancer invasion and metastasis.[5,70−76]

USE OF THE CHORIOALLANTOIC MEMBRANE (CAM) OF CHICK EMBRYOS TO ESTABLISH NANOPARTICLE STABILITY AND QUALIFY NPS FOR *IN VIVO* USE

Nanoparticle stability, defined as prolonged circulation without sequestration by the MPS system and nonspecific binding, is paramount to therapeutic efficiency and to the success of nanoparticle-based imaging and theranostics. For example, in the case of cancer, NP accumulation in the tumor microenvironment relies upon nanoparticle leakage through fenestrations of the cancer vasculature according to the enhanced permeability and retention (EPR) effect,[77−79] NP transcytosis,[80,81] or targeted binding[82,83]—in all cases NPs must remain in circulation for sufficient periods of time to passively or actively accumulate in the tumor. As noted above, the failure of injected NPs to reach/locate solid tumors remains the biggest obstacle to nanomedicine, and we contend that this failing is due to the instability of NPs *in vivo*. In the preponderance of nanomedicine studies, the stability of NPs is assessed *in vitro* using a variety of characterization techniques: dynamic light scattering (DLS) to determine the particle size distribution and polydispersity index in solution, ζ potential to determine particle charge in solution, transmission electron microscopy (TEM) to directly visualize particle size and shape following drying, and occasionally cryogenic electron microscopy (cryo-EM) to image NPs in the appropriate liquid medium. Oftentimes NPs are considered stable if their particle size remains constant over time in physiologically relevant media characterized by high ionic strength, where the Debye length approaches zero and electrostatic stabilization mechanisms are inoperative. It should be noted, however, that hundreds of such studies have been conducted in deionized water, where electrostatic stabilization mechanisms are dominant, and correspondingly the conclusion drawn may not be valid *in vivo*. Further insight into stability has been

https://doi.org/10.1021/acsnano.2c03990
ACS Nano 2022, 16, 19626−19650

gleaned from the meta-analysis of NP delivery efficiency cited above, where the following trends were observed: (1) inorganic materials (e.g., gold NPs or quantum dots) exhibit a higher median delivery efficiency compared to organic materials (e.g., liposomes or polymeric NPs), (2) particles with hydrodynamic diameters <100 nm show a higher median delivery efficiency (in terms of intratumoral fluorescence intensity) than larger particles, and (3) the delivery efficiency of nanoparticles exhibiting neutral ζ potentials, as defined from −10 to 10 mV at pH 7.4, is higher than that of nanoparticles with positive (>10 mV) or negative (←10 mV) ζ potentials.[3] However, size stability per se and trends of delivery efficiency are indirect measures of stability that do not explicitly account for the extents of NP aggregation, NP trapping in the liver, spleen, and lung, rapid uptake by the components of an MPS system, nonspecific binding, and renal clearance—mechanisms inaccessible to *in vitro* investigations that directly inhibit delivery to the tumor or target tissue.

The characteristics of the avian embryo and chorioallantoic membrane models described above, in particular, the ability to inject and image optically labeled NPs in circulation in a highly vascularized living organism possessing an immune system along with target diseased cells, xenograft tumors, etc., enable the direct and immediate assessment of stability and NP half-life. As an example, Movie 1 and Figures 3A,B show the circulation of 150 nm diameter, fluorescent green labeled, polyethylene glycol coated (PEGylated), mesoporous silica nanoparticles (MSNPs) in the CAM vasculature for a period of 1 h after injection. Although the NPs exhibited stability for a period of ∼80 h in distilled H_2O, phosphate buffered saline (PBS), and cell culture media with and without added serum, they show progressive aggregation within the capillaries of the CAM over time that was substantially greater in the venous network as opposed to the arterial network. The instability and accumulation on the vessel walls could be mediated either by circulating immune cells or by strong interaction with the cells of the vasculature, both of which would necessarily reduce NP delivery efficiency to a tumor. Although crucial to delivery efficiency, traditional *in vitro* characterization methods provide little insight regarding this "instability" mechanism, which is immediately visualized in the CAM.

To reduce nonspecific binding and uptake by the immune system and enhance NP biocompatibility, encapsulation of NPs within supported lipid bilayers[84] or native cell membranes[85] has proven to be highly effective. For the case of PEGylated, zwitterionic-supported lipid bilayers, the near neutrally charged hydrophilic surface provides hydration stabilization and helps to prevent opsonization by immunoglobulins, complement proteins, or receptors present on the surface of macrophages, thereby reducing uptake by the MPS or complement systems. As an example, Movie 2 and Figure 3C show the circulation of PEGylated, zwitterionic lipid bilayer encapsulated MSNPs 30 min postinjection into the CAM. Compared to their PEGylated MSNP counterparts (Figure 3A,B), lipid encapsulation confers greater stability, as is immediately evident by the circulation behavior and avoidance of uptake by the MPS system—features impossible to assess *in vitro*. Native cell membranes are similarly zwitterionic, providing hydration stabilization, and further contain markers of self (e.g., CD47) that prevent uptake by macrophages. Movie 3 and Figure 3D show the circulatory behavior of human erythrocyte membrane encapsulated MSNPs in the CAM within several minutes of injection. We observe the

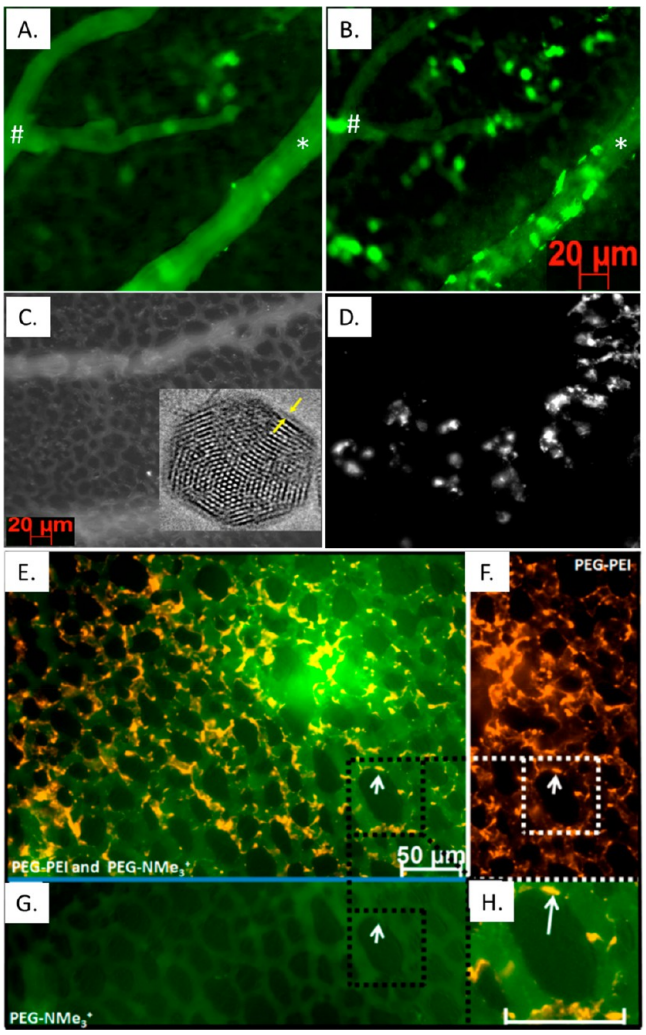

Figure 3. Using intravital microscopy in the CAM to understand nanoparticle behavior. (A, B) Screen captures from a video of 150 nm PEGylated MSNPs in the CAM vasculature over 60 min. The artery is denoted with * and the vein with #. (A) Under 10 min, the MSNPs remain in circulation. (B) By 60 min, the particles have begun to accumulate on the vessel walls in the capillary plexus. (C) MSNPs coated with a lipid bilayer circulating 30 min post-injection. Inset: CryoTEM image of the MSNP with the lipid bilayer highlighted with arrows. Adapted with permission from ref 84. Copyright 2016 American Chemical Society. (D) Human erythrocyte membrane coated MSNPs arrest within the CAM within minutes of injection. Images in (A)−(C) were adapted with permission from ref 222. (E−H) Comparison of the vascular interaction of size and charge-matched MSNPs in the CAM. MSNs coated with PEG-PEI (orange) and PEG-NMe_3^+ (green) were imaged in the CAM 10 min postinjection. Images in (E)−(H) adapted with permission from ref 86. Copyright 2016 American Chemical Society. (E) Merged image, (F) PEG-PEI-coated MSNs arrest on the vessel walls while (G) PEG-NMe^{3+} coated MSNs remain in circulation. (H) Magnification highlighting (arrow) the arrest of PEG-PEI-coated MSNs on the endothelial cells.

MSNPs to be immediately and completely arrested/sequestered by chick embryo blood cells. Here the point is that the CAM MPS system recognizes human red blood cell encapsulated MSNPs as foreign and eliminates them from circulation—thus demonstrating the effectiveness of the CAM MPS and highlighting the utility of imaging in the CAM as a means of evaluating NP stability.

https://doi.org/10.1021/acsnano.2c03990
ACS Nano 2022, 16, 19626−19650

The ability to visualize in real time the behavior of NPs within blood flow via intravital microscopy in the CAM can further facilitate detailed comparisons between NPs for the development of structure versus function relationships. For example, 50 nm MSNPs coated with either polyethylene glycol and polyethylenimine (PEG-PEI) or polyethylene glycol and a quaternary ammonium silane (PEG-NMe_3^+) will have the same average surface charge (+40 mV) and would be deemed equivalent by most characterization methods. However, the charge distribution and exposure of that charge on the NP surface are very different due to the bulky nature of the PEI molecule and the compact nature of the NMe_3^+ molecule.[86] Injection of fluorescently labeled MSNPs with these two surfaces demonstrated vastly different behaviors in the CAM (Figure 3E–H). While the MSNP PEG-NMe_3^+ particles flowed freely within the vasculature, the MSNP PEG-PEI particles interacted with the endothelial cells and arrested along vessel walls.[150] This exploration of the behavior in the CAM suggested that greater circulation was possible with the MSNP PEG-NMe_3^+ particles. When these particles were later tested in mammalian systems, the MSNP PEG-PEI particles were rapidly removed from circulation and accumulated in the liver.[87] In contrast, the MSNP PEG-NMe_3^+ particles remained distributed throughout the body, confirming the predicted behavior gained from CAM studies.

Intravital microscopy in the CAM system has also been used to evaluate biomimetic systems. The creation of artificial red blood cells capable of mimicking the structure and mechanical properties of biological red blood cells is difficult and requires testing in a relevant system. The CAM vasculature allows a direct observation of the behavior of red blood cell mimics in pulsatile flow and the monitoring of any NP entrapment within the capillary bed of the CAM. Intravital microscopy within the CAM was used to demonstrate the creation of long circulating and deformable red blood cell mimics capable of flow within the larger vessels and deformation to move through the capillary bed.[88,89] Due to the low cost of the CAM, an examination of individual steps throughout the process for creation of red blood cell mimics could be performed and compared for compatibility with blood vessels and capillaries to refine the design. When the red blood cell mimics were later tested in a mammalian system, the long circulation times found in the CAM were confirmed.[88]

THE CHICK EMBRYO AND CAM FOR ASSESSING THERAPEUTIC EFFICACY AND IMAGING PERFORMANCE OF NPS

Both the chick embryo and its CAM have been used to test the behavior and biocompatibility of nanomaterials. While the CAM is more commonly utilized, the embryos themselves can be used for a variety of tests (Table 1). The most common test is toxicity to the embryo itself, as assessed by embryo death or low weight. Embryo toxicity has been studied with curcumin-Au NPs,[90] Ag NPs,[91] Cu NPs,[92] nanoparticular iron complexes,[93] superparamagnetic iron oxide NPs,[94] periodic mesoporous organosilica NPs (PMOs),[95] Qdots (CdSe, CdTe/ZnS and CdSe/ZnS),[96] carbon NPs,[97,98] liposomes loaded with 5-aminolevulinic acid and protoporphyrin IX,[99] chitosan,[100] and polylactic-*co*-glycolic acid (PLGA) NPs.[101] In some cases, this basic analysis is coupled with more in-depth studies, including the quantification of embryo defects or blood and organ biochemical studies to increase the understanding of the nanoparticle effects.[93,98,99,102] The ease of use and the low cost of the CE system allow a direct comparison between multiple groups of particles. For example, characterization of the embryo such as body and organ weight and blood and liver biochemistry was used to perform a detailed examination of different carbon NPs, including diamond NPs, graphite NPs, pristine graphene, small graphene oxide, large graphene oxide, and reduced graphene oxide.[98] This study demonstrated no major adverse effects with carbon NPs regardless of the NP type, thereby helping to qualify carbon NPs for *in vivo* use.

Table 1. Nanomaterial Testing in the Avian Embryo

chick embryo	nanoparticles	ref
embryo survival, weight	Au NPs	90
	Ag NPs	91
	Cu NPs	92
	nanoparticular iron complexes	93
	iron oxide NPs	94
	silica NPs	95
	Qdots	96
	carbon NPs	98, 102
	liposomes	99
	polymeric NPs	100, 101
embryo defects	liposomes	99
blood and organ biochemistry	nanoparticular iron complexes	93
	$CoFe_2O_4$, $NiFe_2O_4$, and $MnFe_2O_4$ NPs	142
	carbon NPs	98, 102
molecular analysis of embryo	Cu NPs	92
	carbon black NPs	103
visualization of delivery to embryo	silica NPs	95
	lipid-based NPs	105, 106
	polymeric NPs	107
chick aortic arch assay	chitosan NPs	219
femur ossification	TiO_2 NPs	104

CEs are also amenable to tissue collection and analysis at the completion of an experiment. This has led to the use of CEs for quantification of mRNA from pectoral muscles exposed to Cu NPs to gain an understanding of the effects on signaling factors involving vascularization and exploration of Cu NPs as a proangiogenic agent.[92] In addition to therapeutic evaluations, the CE system can be used to understand the effects of nanomaterials on developing embryos. Chicken embryos were exposed to carbon black NPs, and the mRNA levels of genes associated with oxidative stress, inflammation, and apoptotic pathways in the brain tissue were assessed.[103] The data collected in this study demonstrated the potential for carbon black NPs to increase inflammatory and apoptotic responses in the embryonic brain.[103] The rapid development cycle of the CE can also facilitate a rapid understanding of the effects of nanomaterials on processes such as bone ossification and vessel formation in the heart. CEs were exposed to TiO_2 NPs and nanobelts, which are commonly used in food, cosmetics, and water purification. Due to the rapid growth of the embryo, femurs collected only 7 days post-exposure could be examined for alteration in structure and the TiO_2 nanobelts showed a significant reduction in porous structure in the femur.[104]

In addition to physical and molecular analyses, the small sizes of CEs make them amenable to fluorescence imaging of the embryo after direct or vascular injection of nanoparticles, including PMO,[95] lipid nanoparticles (LNPs),[105,106] and dextran poly lactic acid (PLA) NPs.[107] Fluorescent imaging of the organs using an *in vivo* imaging system (IVIS)

https://doi.org/10.1021/acsnano.2c03990
ACS Nano 2022, 16, 19626–19650

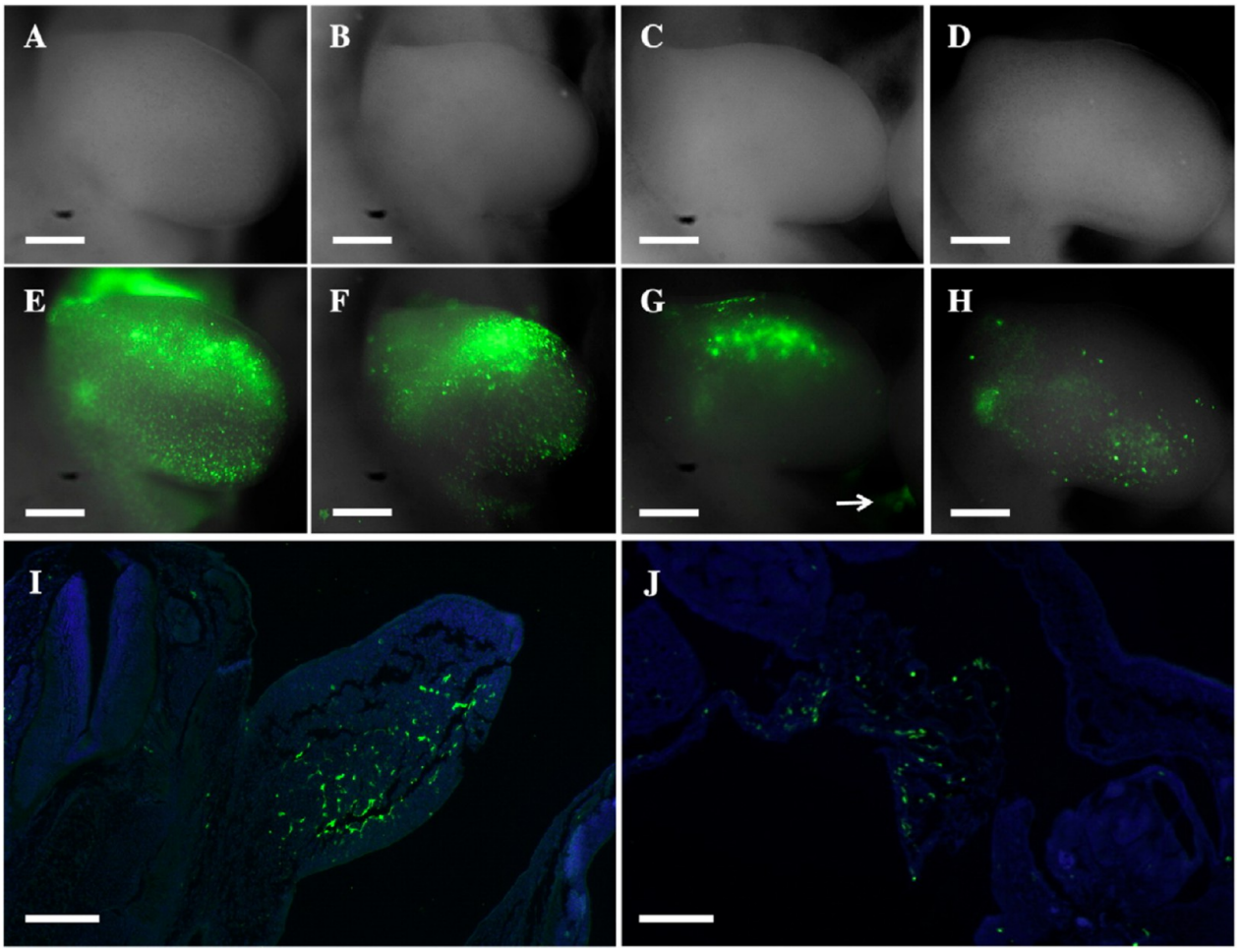

Figure 4. Comparison of plasmid delivery by lipid nanoparticles (LNPa) with different helper lipids. LNPs loaded with a plasmid encoding GFP were directly injected into the forelimb bud of chicken embryos. The efficacy of delivery of LNPs formulated with the helper lipids DOPE (A, E), DOPC (B, F), DSPC (C, G), and SOPC (D, H) were compared using fluorescence microscopy of the intact embryo. The DOPE-based LNPs were the most effective, and imaging thin sections of the embryo forelimb (I) showed delivery throughout the forelimb and vascular infiltration leading to delivery to the heart (J). Reprinted with permission from ref 106. Copyright 2017 Elsevier.

demonstrated no accumulation of the doxorubicin-loaded PMO particles in organs after vascular injection, which, combined with the low overall toxicity of PMO delivery agents, supports the use of PMO particles for cancer therapeutics.[95] CEs have also been used as a rapid method to downselect LNP formulations for nucleic acid delivery (Figure 4). LNPs were formulated with different helper lipids, directly injected into the forelimb of the developing embryo, and imaged the following day.[106] Observation of the intact forelimbs highlights the influence the helper lipid has on the efficacy of LNP delivery, where DOPE showed the most widespread efficacy (Figure 4A,B). Sectioning the forelimb showed that DOPE-based formulations were capable of delivery of plasmids to both internal and surface tissues (Figure 4I). Sectioning of the heart showed incidental delivery into the vasculature that was capable of affecting distal organs (Figure 4J), revealing the potential for vascular delivery of nucleic acids with the DOPE-based LNP formulation.[106]

While the embryo has been used for a variety of studies, most nanomaterial studies using CE systems focus on the CAM due to the ready access to the vasculature and lack of innervation, removing the need for anesthesia (Table 2). The CAM membrane is historically used in the hen's egg-chorioallantoic membrane (HET-CAM) irritation test as an alternative to rabbits for studying vascular irritation caused by chemicals. The HET-CAM test has also been applied to a wide variety of NPs, including 30 and 100 nm superparamagnetic iron oxide NPs,[94,108] silica NPs,[109] nanostructured lipid carriers,[110−112] solid lipid nanoparticles,[113−115] dendritic core multishell nanotransporters,[114] PLGA-based NPs,[116−118] polycaprolactone-based NPs,[119,120] poly(3-hydroxybutyrate-*co*-3-hydroxyvalerate) NPs,[121] poly(HEMA)-based NPs,[122] NPs made from plant polymers,[123] oil nanoemulsions,[124] chitosan-based nanosuspensions,[125] and xyloglucan nanoaggregates.[126] The ease of use of the HET-CAM test facilitated comparisons of various polymer coatings on 100 nm superparamagnetic iron oxide NPs.[94] The CAM and associated embryo were utilized to study the effects of polymer charge (neutral, negative, and positive) and size of both free polymer and polymer applied as an NP coating on hemorrhage, thrombosis, vascular lysis, and embryo death after vascular injection. From these data it was observed that noncharged polymer coated NPs showed only minor thrombosis associated with the smaller blood vessels over time, suggesting a response due to trapping based on particle size. The anionic polymer coated NPs showed more rapid thrombosis than the neutral particles and the polymer with the highest molar mass showed vascular lysis at 24 h. By comparison, the cationic polymer coated NP on injection

https://doi.org/10.1021/acsnano.2c03990
ACS Nano 2022, 16, 19626−19650

Table 2. Nanomaterial Testing in the Chorioallantoic Membrane (CAM)

CAM	nanoparticles	ref
HET-CAM assay for irritation	iron oxide NPs	94, 108
	silica NPs	109
	lipid-based NPs	110−113
	polymeric NPs	116−123
	dendritic core-multishell nanotransporters	114
	nanoemulsions and nanosuspensions	124, 125
	nanoaggregates	126
angiogenesis/ antiangiogenesis	Au NPs	127−133
	Cu NPs	92, 134
	TiO_2 NPs	104
	ZnO NPs	135−137
	selenium NPs	138
	Y_2O_3 NPs	139
	silica NPs	140, 141
	$CoFe_2O_4$, $NiFe_2O_4$, and $MnFe_2O_4$ NPs	142
	carbon Qdots	143
	carbon NPs	97, 102, 144
	liposomes, exosomes, micelles	131, 145−147
	polymeric NPs	101, 148−154, 219
	dendrimers	155−157
	nanoemulsions and nanosuspensions	158−160
	hydroxyapatite NPs	161
blood vessel physical disruption	TiO_2 NPs	220
	liposomes	162−169
	polymeric NPs	170−172, 221
CAM tissue histology	liposomes	162
	lipid-based NPs	113
	polymeric NPs	150
	nanoemulsions and nanosuspensions	158
microscopy in harvested CAM	Ag NPs	222
	liposomes	223
	polymeric NPs	221
Xenograft in CAM	silica NPs	84, 95, 173, 174
	tungsten carbide-cobalt NPs	175
	liposomes	162, 176−178
	polymeric NPs	179−181,203
molecular analysis of CAM	Au NPs	131
	TiO_2 NPs	104
	carbon Qdots	143
	exosomes	131
intravital imaging	virus-like particles	6, 182−184
	Qdots	187
	polystyrene nanospheres	185, 187
	iron oxide NPs	188
	silica NPs	84, 86

resulted in more severe adverse effects. All of the cationic NPs resulted in thrombosis and embolic events, and the higher molar mass polycationic polymer coatings resulted in embryonal death. Interestingly, when the authors compared their data in the CAM system to the *in vitro* assays, they found that while *in vitro* assays alone were sufficient to predict the hemotoxicity of polymers, they were insufficient to predict the hemotoxicity profile for the nanoparticles.[94] This work highlights the utility of the CAM as an efficient alternative to mammalian animal studies.

The most common use of the CAM in nanomaterials studies is in the observation and quantification of the effect on angiogenesis (Table 2). The CAM, with regard to assessing the angiogenic or antiangiogenic properties of nanomaterials, has been applied to Au NPs,[127−129] peptide-conjugated Au NPs,[130−132] therapeutic conjugated Au NPs,[133] Cu NPs,[92,134] TiO_2 NPs,[104] ZnO NPs,[135−137] selenium NPs loaded in chitosan/collagen scaffolds,[138] polycaprolactone scaffolds loaded with Y_2O_3 NPs,[139] therapeutic loaded mesoporous silica NPs (MSNPs),[140] MSNPs in a collagen scaffold,[141] magnetic metal-Fe_2O_4 NPs,[142] carbon Qdots,[143] diamond NPs,[97,102] graphite NPs,[97,102,144] multiwall carbon nanotubes,[97,144] graphene nanosheets,[97] fullerenes,[97,144] liposomes,[145,146] chronic myeloid leukemia cell exosomes,[131] inulin/vitamin E micelles,[147] PLGA NPs,[101,148,149] PLA NPs,[150] polysaccharide NPs,[151,152] chitosan NPs,[153,154] dendrimers,[155−157] therapeutic nanoemulsions,[158−160] and vincristine-loaded hydroxyapatite NPs.[161] Angiogenic studies in the CAM are done for two major reasons, the first being screening of an unexpected or unwanted effect and the second being the active use of the CAM to study therapeutic NPs with planned angiogenic effects. Screening studies revealed dose-responsive inhibition of blood vessel formation with green synthesized Au NPs and ZnO NPs as well as diamond NPs and multiwalled carbon nanotubes.[97,129,135] Blocking angiogenesis is a common target for preventing cancer progression and metastasis. The CAM system provides an easy and quantifiable method to evaluate nanomaterials designed to inhibit angiogenesis. For example, MSNPs targeted to the tumor vasculature using an RGD peptide and loaded with the antiangiogenic drug NAMI-A (imidazolium *trans*-imidazole dimethyl sulfoxide tetrachlororuthenate) showed significant antiangiogenic activity that exceeded the efficacy of the free drug and even blocked direct angiogenesis stimulation via vascular endothelial growth factor (VEGF) addition.[140] The ability of nanoparticles to block proangiogenic signals has also been demonstrated via the CAM with Au NPs. Chronic myeloid leukemia (CML) progression is commonly associated with increased angiogenesis in the bone marrow mediated by exosomes released by the CML cells. The ability of the CML exosomes to increase angiogenesis was demonstrated in the CAM, and then the ability of Au NPs functionalized with antiangiogenic peptides to block this induced angiogenesis was shown.[131] After examining the angiogenic and antiangiogenic effects of the exosomes and peptide-Au NPs, the CAM tissue was harvested and molecular analyses were performed to understand the effects on expression of genes associated with angiogenesis. The molecular analysis demonstrated the effect of both the CML exosomes and peptide-Au NPs in modulating the expression of VEGFR-1 to control angiogenesis.[131] A complementary molecular analysis of the CAM after angiogenesis studies has also been done with TiO_2 NPs and carbon Qdots.[104,143] Histological assessment of the CAM can also be used to supplement angiogenesis studies. These studies often look for changes in or loss of blood vessels and alterations in thickness or structure that indicate a larger effect beyond angiogenesis.[150,158]

https://doi.org/10.1021/acsnano.2c03990
ACS Nano 2022, 16, 19626−19650

Due to the ability to rapidly and clearly visualize blood vessels, the CAM has become a very common model for studying nanoparticles for photodynamic therapy. The phototherapy of liposomes loaded with *m*-tetra(hydroxyphenyl)-chlorin (mTHPC),[162,163] porphycenes,[164,165] and benzoporphyrin derivative monoacid[166−169] have been visualized with the CAM using both bright-field and fluorescence microscopy. Beyond liposomes, PLGA and PLA polymeric NPs loaded with porphyrins and TiO_2 NPs have been assessed for photodynamic therapy potential using the CAM.[170−172] For example, liposomal mTHPC was injected i.v. into the CAM and the therapeutic efficacy of different intervals between liposome injection and light activation was observed (Figure 5).[162] The

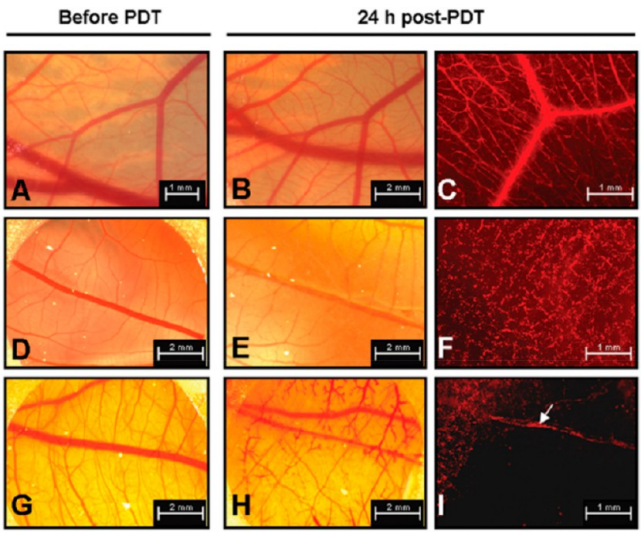

Figure 5. CAM blood vessel response to liposomal mTHPC photodynamic therapy. Liposomal mTHPC was injected i.v. into the CAM and the illuminated with a 652 nm diode laser 15 min (A−C), 1 h (D−-F) and 3 h (G−I) after i.v. injection. Twenty-four hours postillumination, 200 nm fluorescent polystyrene spheres were i.v. injected to highlight the asculature (C, F, I). Reprinted with permission from ref 162. Copyright 2014 Taylor & Francis Ltd.

disruption of the blood vessels 24 h post-treatment was visualized by light microscopy and by using fluorescent microspheres to highlight the vasculature. The visualization showed a dose-dependent disruption, while the fluorescent imaging allowed detection of the loss of blood flow to regions of the CAM by 200 nm polystyrene particle exclusion.[162] The ability to rapidly access the response of blood vessels within 24 h of exposure also facilitates rapid comparisons between formulations. A direct comparison of mTHPC formulations with and without the addition of a PEGylated lipid using vascular disruption in the CAM showed an increase in efficacy by the inclusion of the PEGylated lipid.[162] This same study went on to compare the two formulations in xenograft tumors in the CAM, highlighting another common use of the CAM model.

The vascular nature of the CAM combined with the immature immune system in the early stages of chick embryo development makes the CAM an excellent model system for xenograft studies. As discussed previously, the CAM allows ready visualization of tumor growth and is applicable to a wide variety of tumor systems. CAM xenografts have been applied to PMO NPs in ovarian cancer,[64] MSNPs in thyroid cancer and leukemia,[84,173] MSNP-coated Au nanorods in fibrosarcoma,[174] tungsten carbide-cobalt NPs in lung cancer,[175] liposomes in breast cancer, ovarian cancer, and neuroblastoma,[162,176−178] and PLGA NPs in lung, thyroid, and renal cancers.[179−181] Xenografts on the CAM recruit blood vessels (Figure 6A) and both the tumor and the blood vessels remain visible. This makes the xenograft CAM models ideal for studying both the effects of the NPs on the xenografts and the effects of the NPs on xenograft-induced angiogenesis. Studies of therapeutic nanoparticles on the xenograft itself often focus on tumor volume or weight, which can be easily measured at the end of the study. Studying tumor volume or weight with PLGA NPs loaded with Tetrac has demonstrated control of tumor growth in thyroid, lung, and renal cancer.[179−181] The tumor growth control was then tested in mouse model systems, and, as predicted by the response in the CAM xenograft, tumor growth was limited by Tetrac-loaded PLGA NP therapy.[179−181] In addition to direct measures of tumor size, the CAM xenografts can be collected and studied using histology and immunohistochemistry. Tumor extraction followed by hematoxylin and eosin (H&E) staining demonstrated tumor necrosis in breast cancer xenografts in response to liposomal delivery of mTHPC followed by photodynamic therapy compared to untreated tumors (Figure 6B,C).[162] In addition to basic H&E staining, the CAM xenografts are amenable to more complex immunohistochemistry techniques to facilitate a more complete understanding of the effects of nanomaterials on targeted tumors. The effects of dual-therapeutic-loaded MSNPs on thyroid cancer xenografts was studied in depth using standard H&E staining combined with immunohistochemistry techniques.[173] The treated tumors demonstrated a necrotic phenotype and reduced invasive phenotype compared to treatment with empty MSNPs or the free drug.[173] The ability to easily collect and study xenografts using standard histology and immunofluorescence strengthens the potential use of the CAM system by facilitating detailed studies of tumor response to nanotherapeutics.

Utilizing the CAM xenograft model, PGLA NPs loaded with Tetrac and doxorubicin-loaded liposomes targeted to neovasculature have been demonstrated to reduce xenograft vascularization.[177,178,181] In contrast, tungsten carbide-cobalt NPs induced xenograft angiogenesis, an important finding in understanding the toxic properties of these mixed-metal NPs.[175] The CAM xenograft system can also be utilized for evaluation of highly complex, multimodal nanoparticles. For example, MSNPs containing gold nanorods functionalized with the photosensitizer indocyanine green (ICG), loaded with antivascular therapeutics (doxycycline and fosbretabulin), and then coated with PEG targeted to the tumor endothelium via an RGD-containing peptide were evaluated in a CAM xenograft model.[174] These complex nanoparticles combine three treatment modalities, release of vascular disrupting antiangiogenic drugs via activation by near-infrared (NIR) light to create localized hyperthermia, photothermal therapy through the Au nanorods, and generation of reactive oxygen species through the photosensitizer ICG. CAM fibrosarcoma xenografts with and without NPs were exposed to NIR light and demonstrated vascular disruption mediated by the NPs.[174] Similar to the results comparing xenograft response in the CAM to mammalian models, a demonstration of vascular disruption in the CAM xenograft models predicted therapeutic response in mammalian *in vivo* systems. For example, doxorubicin liposomes targeted to the tumor neovasculature

https://doi.org/10.1021/acsnano.2c03990
ACS Nano 2022, 16, 19626−19650

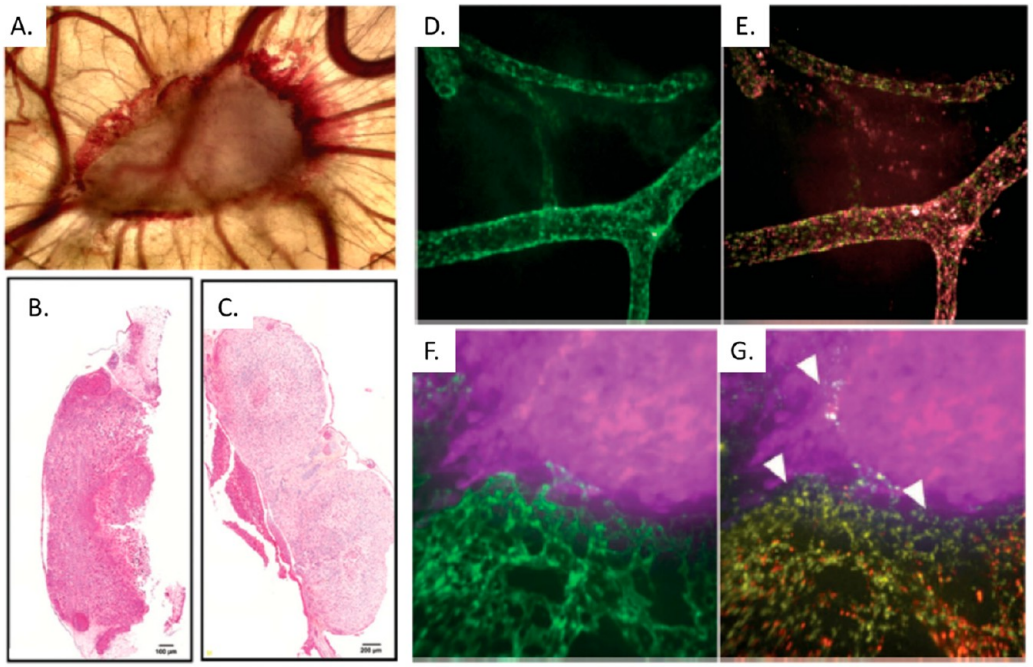

Figure 6. Xenografts in the CAM for nanomaterial studies. (A) Xenografts recruit blood vessels when they are implanted in the CAM. Both the xenograft and the blood vessels can be visualized, allowing a rapid study of the effects of therapeutic nanomaterials targeted to both the tumor and the associated vasculature. (B, C) Tumors can be retrieved from the CAM and studied using common histology techniques such as H&E staining. Untreated breast cancer xenografts show rapid cell proliferation, while tumors treated with liposomes and photodynamic therapy show extensive necrosis. Images in (B) and (C) were reprinted with permission from ref 162. Copyright 2014 Taylor & Francis Ltd. (D, E) Intravital imaging of fluorescently labeled CPMV-based viral nanoparticles which allow direct visualization of the vasculature both immediately (E) and 24 h postinjection (D). (F, G) Intravital imaging can reveal tumor neovascularization. Fibrosarcoma xenograft (magenta) with endothelium labeled with fluoresceine lectin (green) with (G) and without (F) CPMV-based NPs to visualize tumor neovascularization. Images in (A) and (D)−(G) were adapted with permission from ref 6. Copyright 2010 Nature Publishing Group.

which demonstrated vascular disruption to xenograft-induced blood vessels in the CAM resulted in increased survival versus free drug and nontargeted liposomes.[177,178] Together these studies highlight the utility of the CAM xenograft model for studying nanoparticle therapies. The CAM xenograft system can facilitate increased screening of therapeutic NPs more rapidly at a much lower cost than corresponding mouse models.

The thinness and transparency of the CAM also facilitates intravital imaging, which allows direct observations of interactions within the blood vessels using fluorescence microscopy.[6] The direct observation of the system can include the blood vessels and capillary bed, the blood flow, and individual cells injected into the vascular system. Direct observation of the blood vessels and capillary bed can be enhanced by the inclusion of nanomaterials such as cow pea mosaic virus (CPMV) based NPs, which interact with endothelial cells (Figure 6D,E).[6] The interactions of the CPMV-based NPs is strong enough that both long-term (~24 h) and rapid visualization can be performed within the living CAM using these NPs.[6] Furthermore, the bright signal from these fluorescently labeled CPMV-based NPs can be used to visualize neovasculature in xenograft models more easily than with traditional staining methods (Figure 6F,G).[6] The CPMV-based NPs can also be further modified to directly target the neovasculature through the presentation of a peptide on the NP surface targeted to a protein, epidermal growth factor-like domain 7, which is expressed only on endothelial cells undergoing active remodeling.[182] In addition to labeling vasculature, the CPMV-based NPs demonstrate uptake in xenografts, allowing visualization of xenografts directly using intravital microscopy.[183,184] Fluorescent nanoparticles can also be used to enhance the visualization of blood flow within the vessels as well as allow direct visualization of NPs in flow.[185−187] High-speed imaging of the flow of fluorescent NPs within the vessels can be used to facilitate modeling studies of blood flow and of nanoparticles within blood flow.[185,186]

Direct observation of fluorescent NPs within the CAM vasculature increases an understanding of the effects of nanomaterial design choices and environmental factors on NP behavior within biological systems. Superparamagnetic iron oxide nanoparticles (SPIONs) have been proposed as magnetic imaging agents but can be affected by external magnetic fields. Intravital microscopy of fluorescently labeled starch-coated SPIONs demonstrated steady flow within the CAM vasculature in the absence of a magnetic field.[188] When a magnetic field was added, agglomeration and reduced velocity of flow were readily apparent. When the field was removed, there was a partial dissolution of the agglomeration. Interestingly, when the particles were examined in a microfluidic channel, the agglomerates dissolved entirely,[188] highlighting the need to use biological systems to understand the behavior of nanomaterials for biomedical uses.

Intravital microscopy in the CAM can also be used to understand the interactions of cancer cells with the vasculature, such as cancer cell extravasation, a major step in the development of metastasis. Single cells can be imaged and their behavior quantified after injection into the CAM. These direct observations can provide additional insight into the

https://doi.org/10.1021/acsnano.2c03990
ACS Nano 2022, 16, 19626−19650

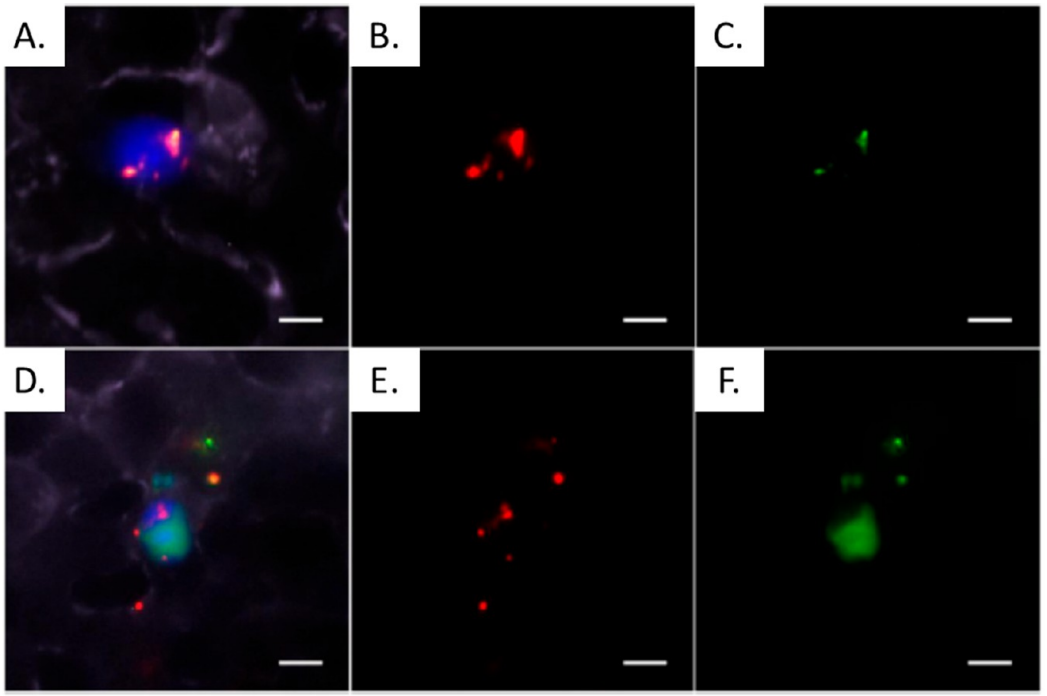

Figure 7. Intravital microscopy showing binding and cargo delivery by antibody-targeted lipid-coated MSNPs to leukemia cells. Leukemia cells were injected into the CAM vasculature and imaged 4 h (A−C) and 16 h post injection (D−F). Fluorescence microscopy showed that the leukemia cells (blue) within the vasculature (lectin vascular stain, lavender) were bound by lipid-coated MSNPs (red) loaded with cell impermeant cargo (YO-PRO-1, green) at 4 h postinjection. By 16 h postinjection, the membrane impermeant cargo has been released from the lipid-coated MSNP within the leukemia cell. Adapted with permission from ref 84.

importance of expressed proteins and the effects of drugs on this important process.[5,71,76] Similarly, the effects of nanoparticles on cancer cells can be directly observed within the CAM. The CAM system was first used to demonstrate the ability of lipid-coated MSNPs (LC-MSNP) with antibody targeting to remain in circulation.[84] Following confirmation that the nanoparticles would remain in circulation, the ability to bind to leukemia cells within the blood was assessed. Leukemia cells were injected into the CAM vasculature followed by injection of fluorescently labeled antibody targeted LC-MSNPs. The targeted LC-MSNPs were able to bind to intravascular cancer cells amidst pulsatile flow and accumulated on the surface of the leukemia cells over time. The addition of a fluorescent cargo to the lipid-coated antibody-targeted MSNPs allowed the observation of binding 4 h postinjection and direct delivery of the fluorescent cargo to the leukemia cell 16 h postinjection (Figure 7).[84]

While the use of intravital imaging in the CAM has been primarily utilized for understanding cancer cell and tumor behavior, there is great potential to use this modality to develop nanomaterials for cancer therapeutics. Intravital imaging has been utilized at a single-cell scale to monitor tumor cell extravasation in three dimensions and at a micrometastasis scale to monitor tumor cell spread over time (Figure 8A,B).[71,189,190] Although these studies often focused on understanding the mechanisms of these processes, these methodologies could be readily translated to the development of nanomaterial therapeutics aimed at reducing metastatic spread. Further, the ability to examine the effects on individual cells can facilitate the development of targeted therapies to the proteins and mechanisms engaged in tumor cell migration. Since the CAM model allows direct cell visualization and vascular injection of chemicals, cancer model cells that can be induced chemically to express fluorescent proteins in response to stimulation can be utilized (Figure 8C).[191] In the CAM, chemically induced expression of E-cadherin could be monitored in real time in extravasated tumor cells and correlated with cell morphology.[191] While this study focused on E-cadherin, a number of model cancer cell lines have been developed for mechanistic studies and most if not all of them could be applied to studies within the CAM. The ability to rapidly translate cell models into the CAM and perform detailed visual analysis in response to nanotherapeutics has the potential to accelerate the development of nanoparticle-based cancer therapies.

THE CAM AND AVIAN EMBRYO AS A TOOL FOR DEVELOPMENT OF NP-BASED CARRIERS AND IMAGING AGENTS

A major area of development for nanomaterials is the development of imaging agents, for both research and clinical diagnostics, and combined therapeutic and diagnostic materials (theranostic agents).[192] In this arena, the chick embryo and its CAM are highly applicable. While optical imaging has limited applications in the clinic for most disease states,[192] optical imaging using fluorescent cells or particles in small animals is a major method in understanding cancer cell behavior and therapeutic development. In the CE, the ability to visualize small metastases of fluorescent melanoma cells to the liver (Figure 8D) and lungs has been demonstrated using a common *in vivo* IVIS.[71] In these studies, melanoma cells expressing fluorescent proteins as markers as well as proteins of interest were vascularly injected. The fluorescent labels allowed quantification of the effect the proteins of interest have on the metastatic potential of the melanoma cells.[71] While this study was focused on the importance of the expression of different

https://doi.org/10.1021/acsnano.2c03990
ACS Nano 2022, 16, 19626−19650

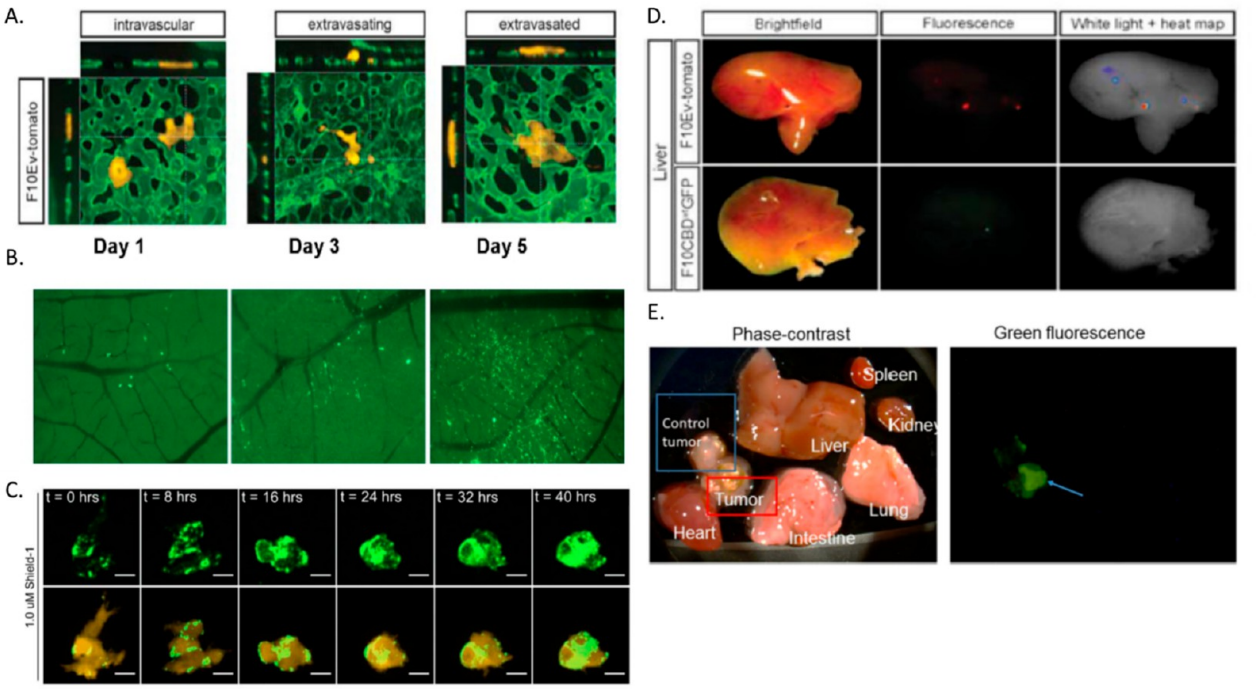

Figure 8. Intravital and fluorescence-based imaging in the CAM, xenografts, and avian embryo. (A) Intravital imaging of single melanoma cells (yellow) extravasating in the CAM capillary network (green). (B) Monitoring the spread of GFP-labeled epidermoid carcinoma micrometastases through the CAM over time. Adapted with permission from ref 189. Copyright 2011 Journal of Visualized Experiments. (C) Monitoring the real-time expression of conditionally expressed E-cadherin (green) in extravasated (yellow) breast cancer cells in response to chemical induction. Images in (C) were reproduced with permission under a Creative Commons CC-BY license from ref 191. (D) Optical imaging of fluorescent metastatic melanoma cells in the liver of the avian embryos 5 days post vascular injection. Images in (A) and (D) were reprinted in part with permission under a Creative Commons CC-BY license from ref 71. (E) Phase contrast and optical imaging of FITC-labeled PMO nanoparticles accumulated in the tumor 3 days post vascular injection. Images in (E) were reproduced with permission under a Creative Commons CC-BY license from ref 95.

proteins, fluorescent cancer cells could also be used to study the therapeutic efficacy of nanoparticles in treating or preventing metastases in the CAM.

Optical imaging of vascular particle delivery has also been tested in the CAM using fluorescein isothiocyanate (FITC) labeled PMO NPs.[95] Lung cancer xenografts were established on the CAM, and after xenograft establishment, the labeled PMO NPs were injected into the vasculature. Three days postinjection the tumors and organs were harvested and optically imaged (Figure 8E).[95] The optical imaging demonstrated significant accumulation of the PMO NPs in the tumor and negligible accumulation in other organs, supporting the use of PMO NPs for tumor-targeted therapeutic delivery. While the studies to date of the chick embryo and CAM for optical imaging have been limited, they demonstrate the potential to utilize the CAM and chick embryo as a rapid way to accelerate nanoparticle development using this common imaging tool. Beyond the optical imaging component for therapeutic development, the chick embryo and CAM are amenable to a wide range of other imaging tools.

One of the clear advantages to the CAM system is the ability to visualize both the xenograft and the associated vasculature without the need for surgery to expose the tumor. This also makes the CAM xenograft model system ideal for technologies that monitor vascular perfusion in real time, such as laser-speckle perfusion imaging (LSPI; Figure 9A).[193] This imaging modality records dynamic blood flow in real time and can reveal tumor hypoxia and angiogenic vessel growth induced by the xenograft. LSPI was used to gain insight into the response of glioblastoma xenografts to antiangiogenic and lactate uptake inhibitors in the CAM.[193] Antiangiogenic treatments in clinical trials have not led to the expected increase in survival and cure for cancer patients and have demonstrated increased metastasis in animal models. One rationale for this has been that antiangiogenic therapies lead to increased tumor hypoxia, which can increase the aggressiveness of the cancer cells. LSPI combined with xenografts on the CAM revealed that antiangiogenic therapy led to a decrease in active angiogenesis, demonstrated by not only a reduced density of vessels around the tumor but also an increase in hypoxia within the xenograft.[193] When a second treatment was added, a lactate uptake blocker, active angiogenesis was reduced without the increase in tumor hypoxia seen with antiangiogenic treatment alone. Further, dual treatment reduced the spread of tumor cells out from the xenograft.[193] While this research focused on drug therapies, this same methodology could be applied to nanomaterials designed to alter angiogenesis or target tumor neovasculature. Furthermore, the easy accessibility of the CAM xenograft models combined with LSPI would allow rapid assessment of the combination of nanotherapeutics with drugs to enhance the effect. Similarly to optical imaging techniques, LSPI combined with xenografts in the CAM provides a rapid way to screen and select promising nanomaterial-based therapeutics.

Xenografts in the CAM have also been studied using ultrasonography. Due to the nondestructive nature of ultrasound measurements, repetitive sonography can be used to monitor tumor growth and vascularization.[194] Xenograft size

https://doi.org/10.1021/acsnano.2c03990
ACS Nano 2022, 16, 19626−19650

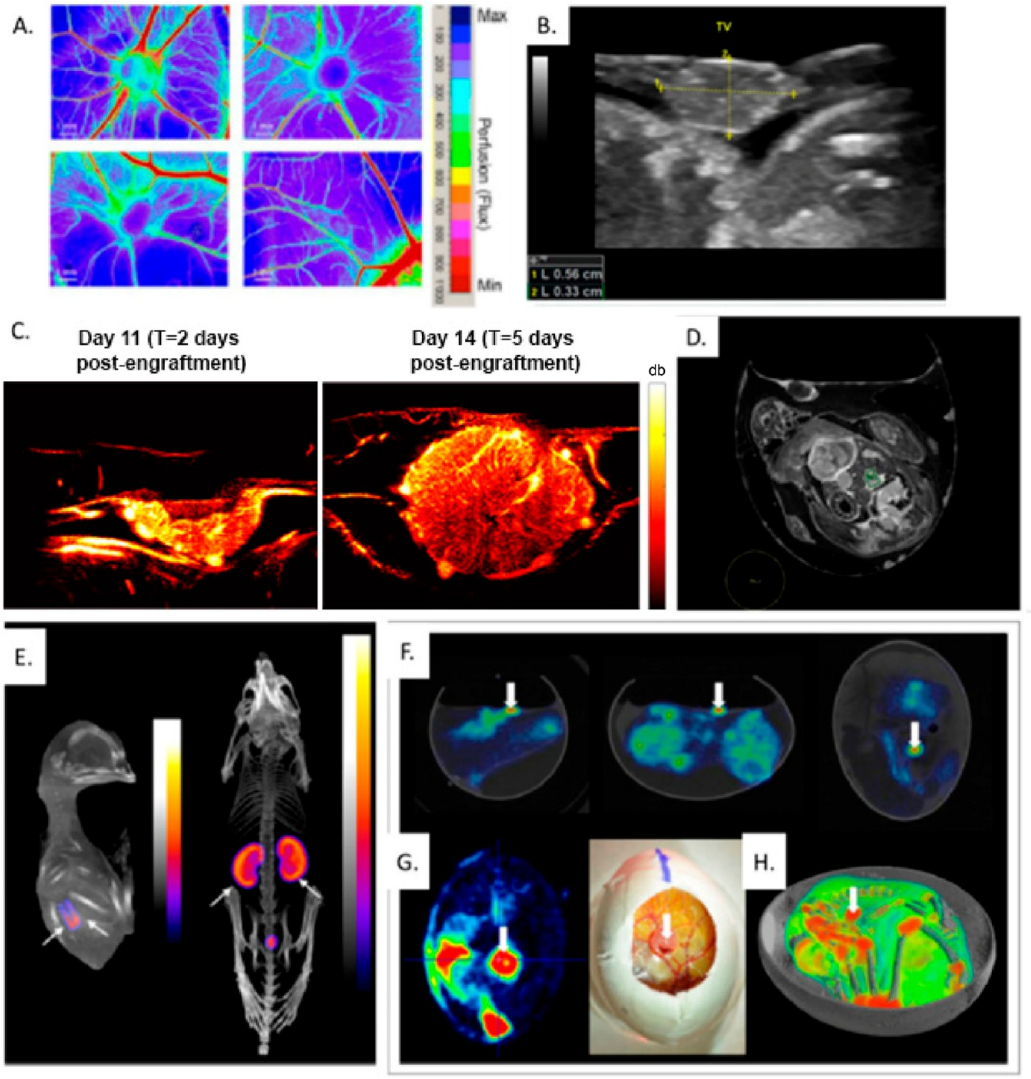

Figure 9. Intravital and fluorescence-based imaging in the CAM, xenografts. and avian embryo. (A) Quantification of tumor perfusion using laser-speckle perfusion imaging (LSPI). Glioblastoma xenografts were imaged without treatment (upper left), treatment with antiangiogenic therapy (upper right), lactate uptake blocker (lower left), or a combination of both therapies. Reprinted with permission under a Creative Commons CC-BY license from ref 193. (B) Ultrasound monitoring of xenograft growth in the CAM. Adapted with permission under a Creative Commons CC-BY license from ref 194. (C) Conventional vascular imaging using ultrasound (left) and optimized ultrasound microvessel imaging (right). Images in (C) were adapted with permission from refs 227 and 228. Copyright 2022 C. Jeffrey Brinker. (D) MRI imaging of chick embryo for development of MRI contrast agents. The liver is highlighted as the region of interest (green), and the background is chosen outside of the egg. Reprinted with permission under a Creative Commons CC-BY license from ref 202. (E) SPECT/CT images of chick embryo and mice after injection of [^{99m}Tc]-DMSA contrast. Arrows highlight the kidneys, demonstrating matching bioaccumulation in chick embryo and mice. Adapted with permission from ref 207. Copyright 2015 Elsevier. (F–H) PET/CT images of the CE and CAM. (F) Two-dimensional coregistered PET and CT images of avian embryo and glioblastoma (arrow) after ^{18}F-FDG injection. (G) Visual comparison of the photographed avian embryo with glioblastoma xenograft and PET/CT image at the level of the CAM. (H) 3D overlay of PET and CT images of ^{18}F-FDG uptake in the embryo and glioblastoma xenograft on the CAM (arrow). Images in (F)–(H) were reprinted with permission from ref 208. Copyright 2013 Journal of Nuclear Medicine.

can be easily measured using ultrasound on the CAM surface (Figure 9B).[194] Tumor growth measurements can be complemented by studies of tumor vascularization using duplex ultrasonography, which looks at the blood flow and vessel structure.[194] Vascular blood flow within CAM xenografts has been evaluated using standard ultrasound Doppler imaging and ultrasound-based microvessel imaging (Figure 9C).[195] Standard ultrasound vasculature imaging has low sensitivity to vessels with slow blood flow, which is common in tumor vasculature. To increase the resolution of microvessels within the xenograft, ultrasound microvessel imaging (UMI) was used to resolve blood flow throughout the xenograft in the CAM (Figure 9C).[195,227,228] The use of UMI was able to differentiate the response of xenograft microvasculature to treatment with antiangiogenic agents and to reveal the development of avascular regions within the xenograft.[195] Ultrasonography is nondestructive to the chick embryos and the CAM, facilitating longitudinal studies for time-resolved response to therapies in both tumor size and vascularization. There is a wide range of nanotherapeutics under development for ultrasound-assisted therapy and imaging,[196−198] and the CAM xenograft models in conjunction with standard ultrasound, duplex ultrasonography,

https://doi.org/10.1021/acsnano.2c03990
ACS Nano 2022, 16, 19626−19650

and UMI imaging could accelerate the development of these imaging and therapy agents.

Magnetic resonance imaging (MRI) has also been applied to avian embryos and CAM xenograft models. MRI imaging can be used to visualize xenografts grown on the CAM and the embryo itself with the use of anesthesia and cooling to facilitate imaging the living embryo.[199] Furthermore, detailed studies of the development of specific organs of interest, such as the brain or eyes, are possible.[200,201] Due to the ability to resolve organs in the living embryos, the chick embryo has been proposed as a model for initial evaluation of contrast agents for MRI.[202] The region of interest, such as the liver, can be selected and compared to a background region outside the egg (Figure 9D) to evaluate promising contrast agents.[202] The chick embryo was utilized to study the effect of dose on contrast enhancement in the liver and umbilical vein and biodistribution of contrast over 40 h postinjection. MRI can also be applied to CAM xenografts and used to evaluate the contrast potential of nanoparticle contrast agents. The distribution of gadolinium tetraazacyclododecanetetraacetic acid (Gd-DOTA) conjugated micelles were compared to standard Gd-DOTA in xenografts in the CAM, demonstrating an increased signal to noise ratio with the micelles.[202] MRI combined with CAM xenografts has also been used to evaluate the localization of a protein-/polymer-based nanoscale theranostic for triple-negative breast cancer. This nanoscale theranostic is composed of albumin and PEG loaded with doxorubicin and labeled with DOTA-Gd to act as an MRI contrast agent.[203] The resulting particles are ∼100 nm in size and were shown to preferentially accumulate in the xenograft tumors implanted within the CAM overtime.[203]

Another interesting use of MRI is the tracking of cells labeled with MRI visible nano- and microparticles over time. SPION-labeled melanoma cells were injected in the neural tube of a chick embryo, and the migration of the cells along the neural crest pathways was followed for 16 days postinjection.[204] Other cell types beyond tumor cells can also be tracked in this manner and mesenchymal stem cells labeled with iron oxide nano-/microparticles implanted in the avian embryo brain were readily trackable by MRI.[205] Interestingly, this study also labeled the mesenchymal stem cells with a fluorescent protein called TdTomato, which allowed coregistration of the location of live cells expressing TdTomato via optical imaging with the MRI scans of the theranostic particles, confirming the retention of the particles within the living cells.[205] While these studies focused on the behavior of cells in the neural tube and brain, CAM xenografts created with cells prelabeled with Gd-based nanoparticles were clearly visible by MRI.[206] Together, these studies suggest that MRI could facilitate tracking of labeled tumor cells migrating from a xenograft on the CAM.

Finally, the chick embryo and its CAM can also be imaged via computed tomography (CT), positron emission tomography (PET), and single photon emission computed tomography (SPECT). The chick embryo has been proposed as an alternate to mouse models for the evaluation of radiopharmaceuticals and was evaluated in a head to head comparison between the two model systems using SPECT/CT imaging (Figure 9E).[207] The comparisons included biodistribution and clearance of multiple radiotracers, including those with expected accumulation in thyroid, bone, and kidneys. For example, the accumulation of [^{99m}Tc]-DMSA was in the kidneys in both avian embryos and mice (Figure 9E) and $^{125}I^-$ accumulated in the thyroid in both species.[207] The data presented in the study supported the use of the chick embryo as a cost-effective equivalent for radiotracer development and studies using SPECT/CT, which could also be applied to nanoparticle-based radio tracers. PET and PET/CT imaging has also been demonstrated in chilled or anesthetized avian embryos.[199] PET/CT imaging using ^{18}F-FDG demonstrated significant uptake in a glioblastoma xenograft on the CAM (Figure 9F−H) as well as a 3D image of the entire chick embryo.[208] These studies support the use of the chick embryo and its CAM for the development of nanoimaging agents and nanotheranostics.

FUTURE APPLICATIONS OF THE CHICK EMBRYO IN NANO-BIO STUDIES

Pursuits of screening candidate NPs can be enhanced in the future by the use of transgenic chick embryos.[209] One key example is the use of the Roslin GFP chicken line, wherein each nucleated cell overexpresses GFP protein.[210] This line could be used to visualize and quantitate the uptake of fluorescently labeled particles in the red−NIR emission range by any cell within the chick embryo. There is a TdTomato version of this line if the NPs being produced can only be labeled with green emission fluorophores.[211] For specific uptake by the nascent immune cells within the embryo, the CSF1R-eGFP and CSF1R-mApple reporter transgenic chicken lines[212] enable studies of NP uptake by immune cells, which would help predict immunogenicity of the same NPs in rodent models.

If screening of NPs in chick embryos requires loss of function or gain of function models, the iCaspase9 surrogate line can be used to form genetically altered chicken lines.[213] This is a laborious technique, since it requires microinjection of the vector into isolated blood cells, followed by an expansion of clones. These clones are then injected along with a chemical that enables recombination into iCaspase9 host embryos. However, the results are strong because 100% of all offspring are genetically altered. The application of this might be the development of mature immune cells that would enable more native studies of NP bioactivity *in vivo*. Another approach is the DDX4 KO chicken line, which has a transcription activator-like effector nuclease (TALEN) expression cassette for customized genetic manipulation.[214] However, the major limitation with these genetic manipulation approaches is that there is no guarantee that transgenesis will occur early in development, as these have only been proven to be effective in adult chickens.

Another emerging tool is 3D printing of holding containers for *ex ovo* chick embryos. There are some 3D-printed materials that enable use of air-breathable plastics so that the CAM can be manipulated for imaging. These would enable easier whole-body imaging such as PET, MRI, and CT imaging. Customizable platforms for imaging of the CAM are very important for achieving high-resolution visualization of NP versus cellular interactions. For instance, we developed a "chick-ubator" which fixes a glass coverslip onto the surface of the CAM, thus immobilizing the tissue and enabling immersion objective based microscopy (Figure 1E in ref 5 and Figure 3E in ref 76). The chick-ubator facilitates the high-resolution imaging of cancer cell metastasis (Figure 9A), NPs in the vasculature (Figure 4), and NP interactions with target cells (Figure 8).

https://doi.org/10.1021/acsnano.2c03990
ACS Nano 2022, 16, 19626−19650

Table 3. Comparison of CAM versus Other Models for Nano-Bio Studies

	Human	Chick Embryo	2D culture	3D culture	Microfluidic Chips	Zebrafish	Mice	Rats	Primates
Cost	$$$$	$	$	$-$$	$-$$	$$	$$-$$$	$$-$$$	$$$$
Ease	Difficult	Easy	Easy	Medium	Medium	Easy	Medium	Medium	Difficult
Need for REB	Yes	No	No	No	No	No	No	No	No
Orthotopic Tumor Formation	Yes	No				Yes	Yes	Yes	Yes
Heterotopic Tumor Formation		Yes				Yes	Yes	Yes	Yes
Metastasis Formation	Yes	Yes	No	No	No	Yes	Yes	Yes	Yes
Pharmacodynamics	Yes	Yes	No	No	No	Yes	Yes	Yes	Yes
Pharmacokinetics	Yes	Yes	No	No	No	Yes	Yes	Yes	Yes
Serum Half-Life	Yes	Yes	Yes	Yes	Yes	No	Yes	Yes	Yes
Interaction with Stromal Cells	*in vitro*	Yes	Yes	Yes	Yes	Yes	Yes	Yes	Yes
Interaction with Endothelial Cells	*in vitro*	Yes	Yes	Yes	Yes	Yes	Yes	Yes	Yes
Intravital Imaging		Yes			Yes	Yes	Yes	Yes	Yes
Microscopic Imaging of NP	*in vitro*	Yes	Yes	Yes	Yes	Yes	Yes	Yes	Yes
Human Physiologic Conditions	Yes	Yes	Yes	Yes	Yes	No	Yes	Yes	Yes

Moving forward, a means of reliably and easily microinjecting NPs and other chemicals intravenously is desperately needed. The technique of intravenous injection (as described in refs 6 and 76) requires significant training and is critical for nano-bio studies with the CAM. This is more straightforward with rodent models, due to the ubiquity of tail vein injection. However, learning to do both techniques requires the same amount of training and effort. In order to increase the utility of chick embryos for nano-bio studies, devices that enable microinjection will need to be developed. Ideally, this would be coupled to surface of the CAM and induce minimal blood coagulation, similar to implantable vascular ports used in mammalian models. This would enable longitudinal studies wherein NPs/chemicals are released into the circulation at various time points.

While the CE and CAM have many uses in evaluating NPs for biomedical use and there are many improvements currently underway in this model, there are some unknowns and limitations as well. Some of these limitations have to do with the model itself; due to the nature of the CE model, the studies must be relatively short term compared to rodent models. Although the effects of many drugs and nanotherapeutics can be observed in the 2−3-week time frame allowed by the CE and CAM, studies focused on long-term effects and acquired resistance will require modification, such as preconditioning the cells to acquire resistance before grafting, to utilize the CE model. As the embryo is also developing over time, studies that focus on specific organs or the immune system will require testing and validation to determine if there is a preferred time frame in development for the study or if this model system is appropriate at all. Additionally, the CE is an avian model; thus, there are differences in proteins and organs from humans. This could be critical if a specific interaction is targeted, such as an antibody or enzyme expressed in the ECM, vasculature, or target organ. For example, the use of a human erythrocyte membrane to encapsulate MSNPs resulted in rapid sequestration by chick embryo blood cells in the CAM (Movie 3 and Figure 3D). This interaction is likely mediated by a mismatch between human and avian proteins and highlights the potential for mismatch to affect NP behavior. In the case of the ECM and vasculature present in the stroma, some of the proteome has been mapped; therefore, a verification of the target presence may be possible.[215] Additionally, if a particular cell type not present in the CAM is needed in tumor stroma, cografting stromal cells with tumor cells can be a potential solution.[67]

An area specific to NP interaction where differences between mammalian and avian proteins could present an issue is the development of a "protein corona" around the NP. In any physiological environment, proteins adsorb to the surface of NPs. This protein corona changes over time and can have profound effects on pharmacokinetics, tissue accumulation, and toxicity of nanomaterials.[216,217] The protein corona has had only limited studied in avian systems. Interactions between TiO_2 NPs and CE albumin demonstrated protein adsorption to the NP surface forming a protein corona.[218] A more relevant study has also been performed with vascular exposure. Recovery of LC-MSNP from the CAM vasculature after circulating for 30 min showed an increase in size of 9%, with further increases in size with additional circulation time of up to 23% at 240 min.[84] This size increase demonstrates the presence of a protein corona that can change over time in CAM vasculature. While these studies have confirmed that protein coronas are formed when NPs interact with the CE and CAM, no study has yet looked at the composition of the protein corona and if it is representative of the protein corona that forms in mammalian models or humans.

Overall, the chick embryo and its CAM offer a multitude of opportunities for studying nano-bio interactions *in vivo* while foregoing the major costs associated with rodent models and minimizing rodent euthanasia (Table 3). While mouse models when used to study NP interactions with vessels offer invaluable spatial information, they can be costly and underpowered.[224,225] Although the CAM is a seldom used model, the qualities and advantages provided should make the CAM an attractive model for pharmacokinetic and pharmacodynamic studies. This preclinical model can provide rapid screening of NP behavior under physiologically relevant

https://doi.org/10.1021/acsnano.2c03990
ACS Nano 2022, 16, 19626−19650

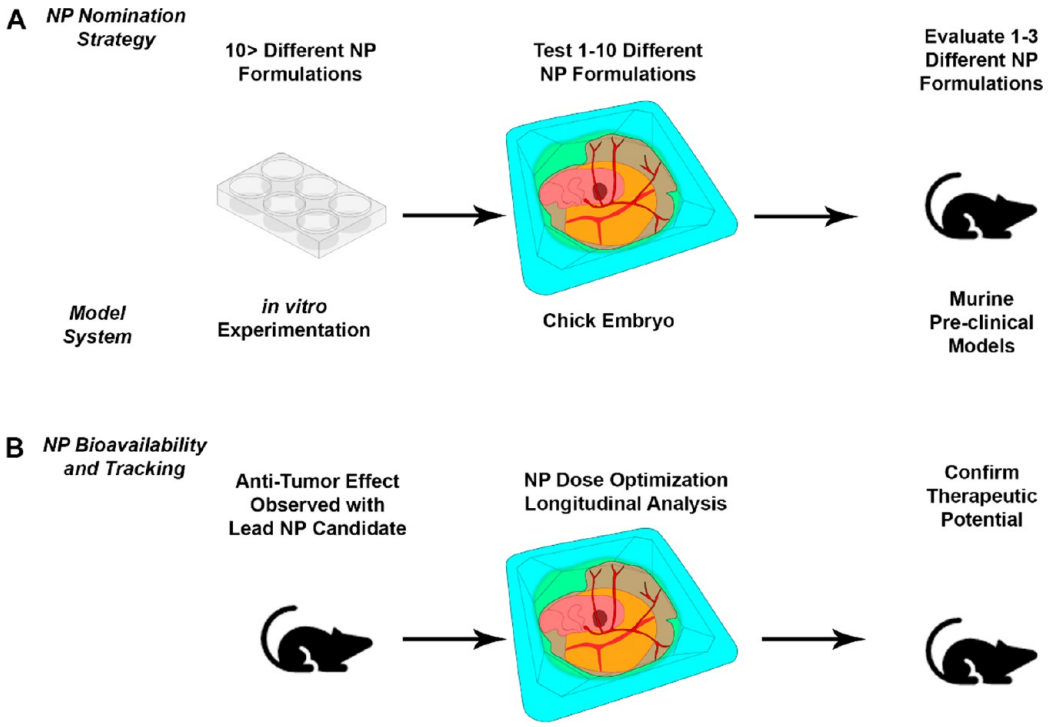

Figure 10. Role of the chick embryo (CE) model for bridging experimental efforts toward clinical modeling of NPs. (A) The CE can be a cost-effective, humane, and rapid means of evaluating many NP candidates prior to experimentation in rodent models. (B) The CE can also be used to optimize the dose for a lead candidate NP that already has a known antitumor effect. The CE offers the ability to perform longitudinal imaging of NP distribution at a low cost for various NP concentrations. After optimization, the determined dose can then be applied in rodent models to confirm therapeutic potential. Image of culture plate adapted with permission under a Creative Commons CC-BY license from ref 226. Copyright 2020 TOGO.

conditions, becoming a rapid, accessible, economical, and more ethical means of qualifying nanoparticles serving as a bridge between *in vitro* assessments and rodent *in vivo* studies. As shown in Figure 10, the CAM can act as an intermediate preclinical model that would assist investigators in their NP nomination strategy as they reduce their NP candidate pool to a smaller pool for *in vivo* analysis in rodent models (Figure 10A). It can also be used to optimize dosing of a lead candidate NP that has initial promise in terms of antitumor efficacy. When the CE is used in this way, dosing of NP across a large range of concentrations can be performed at a low cost. Moreover, extensive longitudinal analyses can be performed within the first 12 h of dose administration (Figure 10B). When an optimal dose is determined, it can then be applied in rodent models again to confirm the same antitumor effect. With these capabilities offered by the chick embryo, we envision its use to become more widespread as nano-bio studies become increasingly fraught with cost, visualization, and ethical issues.

ASSOCIATED CONTENT

Supporting Information

The Supporting Information is available free of charge at https://pubs.acs.org/doi/10.1021/acsnano.2c03990.

Circulation of 150 nm diameter, fluorescent green labeled, polyethylene glycol coated (PEGylated), mesoporous silica nanoparticles (MSNPs) in the CAM vasculature (MOV)

Circulation of PEGylated, zwitterionic, lipid bilayer encapsulated MSNPs (MOV)

Circulatory behavior of human erythrocyte membrane encapsulated MSNPs in the CAM (MOV)

AUTHOR INFORMATION

Corresponding Author

Hon Sing Leong − *Department of Medical Biophysics, Faculty of Medicine, University of Toronto, Toronto M5G 1L7, Canada; Biological Sciences Platform, Sunnybrook Hospital, Toronto M4N 3M5, Canada;* orcid.org/0000-0001-7801-1402; Phone: 416-480-6100 ext.5748; Email: hon.leong@sri.utoronto.ca

Authors

Kimberly S. Butler − *Molecular and Microbiology, Sandia National Laboratories, Albuquerque, New Mexico 87123, United States;* orcid.org/0000-0001-6045-8636

C. Jeffrey Brinker − *Department of Chemical and Biological Engineering and the Comprehensive Cancer Center, The University of New Mexico, Albuquerque, New Mexico 87131, United States;* orcid.org/0000-0002-7145-9324

Complete contact information is available at: https://pubs.acs.org/10.1021/acsnano.2c03990

Notes

The authors declare no competing financial interest.

ACKNOWLEDGMENTS

C.J.B. acknowledges support from the NIH RO1 (FP0003261 and CA226537). K.S.B. was supported by the Laboratory Directed Research and Development Program at Sandia National Laboratories. Sandia National Laboratories is a

multimission laboratory managed and operated by National Technology and Engineering Solutions of Sandia, LLC, a wholly owned subsidiary of Honeywell International, Inc., for the U.S. Department of Energy's National Nuclear Security Administration under contract DE-NA-0003525. The views expressed in this article do not necessarily represent the views of the U.S. Department of Energy or the United States Government. H.S.L. acknowledges Sara Mar, Justin Xu, and Emmanuel Cherin for their contributions for figures in this work.

REFERENCES

(1) Faria, M.; Björnmalm, M.; Thurecht, K. J.; Kent, S. J.; Parton, R. G.; Kavallaris, M.; Johnston, A. P. R.; Gooding, J. J.; Corrie, S. R.; Boyd, B. J.; Thordarson, P.; Whittaker, A. K.; Stevens, M. M.; Prestidge, C. A.; Porter, C. J. H.; Parak, W. J.; Davis, T. P.; Crampin, E. J.; Caruso, F. Minimum information reporting in bio-nano experimental literature. *Nat. Nanotechnol.* **2018**, *13*, 777−785.

(2) Leong, H.-S.; Butler, K. S.; Brinker, C. J.; Azzawi, M.; Conlan, S.; Dufés, C.; Owen, A.; Rannard, S.; Scott, C.; Chen, C.; Dobrovolskaia, M. A.; Kozlov, S. V.; Prina-Mello, A.; Schmid, R.; Wick, P.; Caputo, F.; Boisseau, P.; Crist, R. M.; McNeil, S. E.; Fadeel, B.; Tran, L.; Hansen, S. F.; Hartmann, N. B.; Clausen, L. P. W.; Skjolding, L. M.; Baun, A.; Ågerstrand, M.; Gu, Z.; Lamprou, D. A.; Hoskins, C.; Huang, L.; Song, W.; Cao, H.; Liu, X.; Jandt, K. D.; Jiang, W.; Kim, B. Y. S.; Wheeler, K. E.; Chetwynd, A. J.; Lynch, I.; Moghimi, S. M.; Nel, A.; Xia, T.; Weiss, P. S.; Sarmento, B.; das Neves, J.; Santos, H. A.; Santos, L.; Mitragotri, S.; Little, S.; Peer, D.; Amiji, M. M.; Alonso, M. J.; Petri-Fink, A.; Balog, S.; Lee, A.; Drasler, B.; Rothen-Rutishauser, B.; Wilhelm, S.; Acar, H.; Harrison, R. G.; Mao, C.; Mukherjee, P.; Ramesh, R.; McNally, L. R.; Busatto, S.; Wolfram, J.; Bergese, P.; Ferrari, M.; Fang, R. H.; Zhang, L.; Zheng, J.; Chuanqi, P.; Du, B.; Yu, M.; Charron, D. M.; Zheng, G.; Pastore, C. On the issue of transparency and reproducibility in nanomedicine. *Nat. Nanotechnol.* **2019**, *14*, 629−635.

(3) Wilhelm, S.; Tavares, A. J.; Dai, Q.; Ohta, S.; Audet, J.; Dvorak, H. F.; Chan, W. C. W. Analysis of nanoparticle delivery to tumour. *Nature Reviews Materials* **2016**, *1*, 16014.

(4) Carbone, L. Estimating mouse and rat use in American laboratories by extrapolation from Animal Welfare Act-regulated species. *Sci. Rep.* **2021**, *11*, 493.

(5) Leong, H.-S.; Chambers, A. F.; Lewis, J. D. Assessing Cancer Cell Migration and Metastatic Growth In Vivo in the Chick Embryo Using Fluorescence Intravital Imaging. *Methods Mol. Biol.* **2012**, *872*, 1−14.

(6) Leong, H.-S.; Steinmetz, N. F.; Ablack, A.; Destito, G.; Zijlstra, A.; Stuhlmann, H.; Manchester, M.; Lewis, J. D. Intravital imaging of embryonic and tumor neovasculature using viral nanoparticles. *Nat. Protoc.* **2010**, *5*, 1406−1417.

(7) Tannenbaum, J.; Bennett, B. T. Russell and Burch's 3Rs Then and Now: The Need for Clarity in Definition and Purpose. *Journal of the American Association for Laboratory Animal Science* **2015**, *54*, 120−132.

(8) Nath, S.; Devi, G. R. Three-dimensional culture systems in cancer research: Focus on tumor spheroid model. *Pharmacology & Therapuetics* **2016**, *163*, 94−108.

(9) Mapanao, A. K.; Voliani, V. Three-dimensional tumor models: Promoting breakthroughs in nanotheranosticstranslational research. *Applied Materials Today* **2020**, *19*, 100552.

(10) Ravi, M.; Paramesh, V.; Kaviya, S. R.; Anuradha, E.; Solomon, F. D. P. 3D Cell Culture Systems: Advantages and Applications. *Journal of Cellular Physiology* **2015**, *230*, 16−26.

(11) Bassi, G.; Panseri, S.; Dozio, S. M.; Sandri, M.; Campodoni, E.; Dapporto, M.; Sprio, S.; Tampieri, A.; Montesi, M. Scaffold.based 3D cellular models mimicking the heterogeneity of osteosarcoma stem cell niche. *Sci. Rep.* **2020**, *10*, 22294.

(12) Castiaux, A. D.; Spence, D. M.; Martin, R. S. Review of 3D cell culture with analysis in microfluidic systems. *Analytical Methods* **2019**, *11*, 4220−4232.

(13) Zheng, F.; Fu, F.; Cheng, Y.; Wang, C.; Zhao, Y.; Gu, Z. Organ-on-a-Chip Systems: Microengineering to Biomimic Living Systems. *small* **2016**, *12*, 2253−2282.

(14) Zhang, B.; Korolj, A.; Lai, B. F. L.; Radisic, M. Advances in organ-on-a-chip engineering. *Nature Reviews Materials* **2018**, *3*, 257−278.

(15) Low, L. A.; Mummery, C.; Berridge, B. R.; Austin, C. P.; Tagle, D. A. Organs- on- chips: into the next decade. *Nat. Rev. Drug Discovery* **2021**, *20*, 345−361.

(16) Ahn, S. I.; Sei, Y. J.; Park, H.-J.; Kim, J.; Ryu, Y.; Choi, J. J.; Sung, H.-J.; MacDonald, T. J.; Levey, A. I.; Kim, Y. Microengineered human blood-brain barrier platform for understanding nanoparticle transport mechanisms. *Nat. Commun.* **2020**, *11*, 175.

(17) Gao, G.; Park, W.; Kim, B. S.; Ahn, M.; Chae, S.; Cho, W.-W.; Kim, J.; Lee, J. Y.; Jang, J.; Cho, D.-W. Construction of a Novel In Vitro Atherosclerotic Model from Geometry-Tunable Artery Equivalents Engineered via In-Bath Coaxial Cell Printing. *Adv. Funct. Mater.* **2021**, *31*, 2008878.

(18) Chacko, A.-M.; Han, J.; Greineder, C. F.; Zern, B. J.; Mikitsh, J. L.; Nayak, M.; Menon, D.; Johnston, I. H.; Poncz, M.; Eckmann, D. M.; Davies, P. F.; Muzykantov, V. R. Collaborative Enhancement of Endothelial Targeting of Nanocarriers by Modulating Platelet-Endothelial Cell Adhesion Molecule-1/CD31 Epitope Engagement. *ACS Nano* **2015**, *9*, 6785−6793.

(19) Shuvaev, V. V.; Ilies, M. A.; Simone, E.; Zaitsev, S.; Kim, Y.; Cai, S.; Mahmud, A.; Dziubla, T.; Muro, S.; Discher, D. E.; Muzykantov, V. R. Endothelial Targeting of Antibody-Decorated Polymeric Filomicelles. *ACS Nano* **2011**, *5*, 6991−6999.

(20) Setyawati, M. I.; Tay, C. Y.; Bay, B. H.; Leong, D. T. Gold Nanoparticles Induced Endothelial Leakiness Depends on Particle Size and Endothelial Cell Origin. *ACS Nano* **2017**, *11*, 5020−5030.

(21) Setyawati, M. I.; Mochalin, V. N.; Leong, D. T. Tuning Endothelial Permeability with Functionalized Nanodiamonds. *ACS Nano* **2016**, *10*, 1170−1181.

(22) Tay, C. Y.; Setyawati, M. I.; Leong, D. T. Nanoparticle Density: A Critical Biophysical Regulator of Endothelial Permeability. *ACS Nano* **2017**, *11*, 2764−2772.

(23) Storey, K. The chick embryo revealed. *Trends in Genetics* **1998**, *14*, 209.

(24) Bellairs, R.; Osmond, M. *Atlas of Chick Development*, 3rd ed.; Academic Press: New York, 2014; Vol. *1*, pp 1−692.

(25) Wilting, J.; Papoutsi, M.; Othman-Hassan, K.; Rodriguez-Niedenführ, M.; Prols, F.; Tomarev, S. I.; Eichmann, A. Development of the Avian Lymphatic System. *Microscopy Research and Technique* **2001**, *55*, 81−91.

(26) Khalil, M.; Sultana, S. Z.; Rahman, M.; Mannan, S.; Ahmed, S.; Ara, Z. G.; Sultana, Z. R.; Chowdhury, A. I. Study of prenatal and postnatal development of spleen of Gallus domesticus (deshi chicken). *Mymensingh Medical Journal* **2009**, *18*, 169−174.

(27) Suksaweang, S.; Lin, C.-M.; Jiang, T.-X.; Hughes, M. W.; Widelitz, R. B.; Chuong, C.-M. Morphogenesis of chicken liver: identification of localized growth zones and the role of h-catenin/Wnt in size regulation. *Dev. Biol.* **2004**, *266*, 109−122.

(28) Wakai, S.; Hirokawa, N. Development of the Blood-Brain Barrier to Horseradish Peroxidase in the Chick Embryo. *Cell Tissue Res.* **1978**, *195*, 195−203.

(29) Guyot, N.; Réhault-Godbert, S.; Slugocki, C.; Harichaux, G.; Labas, V.; Helloin, E.; Nys, Y. Characterization of egg white antibacterial properties during the first half of incubation: A comparative study between embryonated and unfertilized eggs. *Poultry Science* **2016**, *95*, 2956−2970.

(30) Garcia, P.; Wang, Y.; Viallet, J.; Jilkova, Z. M. The Chicken Embryo Model: A Novel and Relevant Model for Immune-Based Studies. *Frontiers in Immunology* **2021**, *12*, 791081.

(31) Victorelli, F. D.; de Oliveira Cardoso, V. M.; Ferreira, N. N.; Calixto, G. M. F.; Fontana, C. R.; Baltazar, F.; Gremião, M. P. D.;

https://doi.org/10.1021/acsnano.2c03990
ACS Nano 2022, 16, 19626−19650

Chorilli, M. Chick embryo chorioallantoic membrane as a suitable in vivo model to evaluate drug delivery systems for cancer treatment: A review. *Eur. J. Pharm. Biopharm.* **2020**, *153*, 273−284.
(32) Wachholz, G. E.; Rengel, B. D.; Vargesson, N.; Fraga, L. R. From the Farm to the Lab: How Chicken Embryos Contribute to the Feild of Teratology. *Frontiers in Genetics* **2021**, *12*, 666726.
(33) Vilches-Moure, J. G. Embryonic Chicken (*Gallus gallus domesticus*) as a Model of Cardiac Biology and Development. *Comparative Medicine* **2019**, *69*, 184−203.
(34) Davey, M. G.; Towers, M.; Vargesson, N.; Tickle, C. The chick limb: embryology, genetics and teratology. *International Journal of Developmental Biology* **2018**, *62*, 85−95.
(35) Flentke, G. R.; Smith, S. M. The Avian Embryo as a Model for Fetal Alcohol Spectrum Disorders. *Biochemistry and Cell Biology* **2018**, *96*, 98−106.
(36) Vargas, A.; Zeisser-Labouèbe, M.; Lange, N.; Gurny, R.; Delie, F. The chick embryo and its chorioallantoic membrane (CAM) for the in vivo evaluation of drug delivery systems. *Adv. Drug Delivery Rev.* **2007**, *59*, 1162−1176.
(37) Fonseca, B. B.; da Silva, M. V.; de Morais Ribeiro, L. N. The chicken embryo as an in vivo experimental model for drug testing: Advantages and limitations. *Lab Animal* **2021**, *50*, 138−141.
(38) Kue, C. S.; Tan, K. Y.; Lam, M. L.; Lee, H. B. Chick embryo chorioallantoic membrane (CAM): an alternative predictive model in acute toxicological studies for anti-cancer drugs. *Experimental Animals* **2015**, *64*, 129−138.
(39) Field, L. H.; Headley, V. L.; Underwood, J. L.; Payne, S. M.; Berry, L. J. The Chicken Embryo as a Model for Campylobacter Invasion: Comparative Virulence of Human Isolates of *Campylobacter jejuni* and *Campylobacter coli*. *Infect. Immun.* **1986**, *54*, 118−125.
(40) Jacobsen, I. D.; Große, K.; Slesiona, S.; Hube, B.; Berndt, A.; Brock, M. Embryonated Eggs as an Alternative Infection Model to Investigate *Aspergillus fumigatus* Virulence. *Infect. Immun.* **2010**, *78*, 2995−3006.
(41) King, V.; Bavetsia, A.; Bumstead, N. Effect of host lineage on the virulence of *Campylobacter jejuni/coli* in the chick embryo model. *FEMS Microbiology Letters* **1993**, *106*, 271−274.
(42) García-Gareta, E.; Binkowska, J.; Kohli, N.; Sharma, V. Towards the Development of a Novel Ex Ovo Model of Infection to Pre-Screen Biomaterials Intended for Treating Chronic Wounds. *Journal of Functional Biomaterials* **2020**, *11*, 37.
(43) Adam, R.; Mussa, S.; Lindemann, D.; Oelschlaeger, T. A.; Deadman, M.; Ferguson, D. J. P.; Moxon, R.; Schroten, H. The avian chorioallantoic membrane in ovo - a useful model for bacterial invasion assays. *International Journal of Medical Microbiology* **2002**, *292*, 267−275.
(44) Maibier, M.; Reglin, B.; Nitzsche, B.; Xiang, W.; Rong, W. W.; Hoffman, B.; Djonov, V.; Secomb, T. W.; Pries, A. R. Structure and Hemodynamics of Vascular Networks in the Chorioallantoic Membrane of the Chicken. *American journal of physiology - heart and circulatory physiology* **2016**, *311*, H913−H926.
(45) Merckx, G.; Tay, H.; Lo Monaco, M.; van Zandvoort, M.; De Spiegelaere, W.; Lambrchts, I.; Bronckaers, A. Chorioallantoic Membrane Assay as Model for Angiogenesis in Tissue Engineering: Focus on Stem Cells. *Tissue Engineering: Part B* **2020**, *26*, 519−539.
(46) Budai, P.; Kormos, E.; Buda, I.; Somody, G.; Lehel, J. Comparative evaluation of the HET-CAM and ICE methods for objective assessment of ocular irritation caused by selected pesticide products. *Toxicology In Vitro* **2021**, *74*, 105150.
(47) Aventurado, C. A.; Billones, J. B.; Vasquez, R. D.; Castillo, A. L. In Ovo and In Silico Evaluation of the Anti-Angiogenic Potential of Syringin. *Drug Design, Development and Therapy* **2020**, *14*, 5189−5204.
(48) Kachooei, S. A.; Rahmani, R.; Zareh, N.; Donyadideh, F.; Kachooei, S. A.; Nabiuni, M.; Yazdansetad, S. Down-regulation of TGF-β, VEGF, and bFGF in vascular endothelial cells ofchicken induced by a brittle star (Ophiocoma erinaceus) extract. *Heliyon* **2020**, *6*, e03199.
(49) D'Arcy, P. F.; Howard, E. M. A new Anti-Inflammatory test, utilizing the chorio-allantoic membrane of the chick embryo. *British Journal of Pharmacology and Chemotherapy* **1967**, *29*, 378−387.
(50) Ma, Y.; Jin, X.-B.; Chu, F.-J.; Mei Bao, D.; Zhu, J.-Y. Expression of liver-targeting peptide modified recombinant human endostatin and preliminary study of its biological activities. *Appl. Microbiol. Biotechnol.* **2014**, *98*, 7923−7933.
(51) Debefve, E.; Pegaz, B.; van den Bergh, H.; Wagnières, G.; Lange, N.; Ballini, J.-P. Video monitoring of neovessel occlusion induced by photodynamic therapy with verteporfin (Visudyne), in the CAM model. *Angiogenesis* **2008**, *11*, 235−243.
(52) Grambow, E.; Sorg, H.; Sorg, C. G. G.; Strüder, D. Experimental Models to Study Skin Wound Healing with a Focus on Angiogenesis. *Medical Sciences* **2021**, *9*, 55.
(53) Ahanger, A. A.; Prawez, S.; Kumar, D.; Prasad, R.; Amarpal; Tandan, S. K.; Kumar, D. Wound healing activity of carbon monoxide liberated from CO-releasing molecule (CO-RM). *Naunyn-Schmiedeberg's Archives of Pharmacology* **2011**, *384*, 93−102.
(54) Talekar, Y. P.; Apte, K. G.; Paygude, S. V.; Tondare, P. R.; Parab, P. B. Studies on wound healing potential of polyherbal formulation using in vitro and in vivo assays. *Journal of Ayurveda and Integrative Medicine* **2017**, *8*, 73−81.
(55) Buzzá, H. H.; Silva, L. V.; Moriyama, L. T.; Bagnato, V. S.; Kurachi, C. Evaluation of vascular effect of Photodynamic Therapy in chorioallantoic membrane using different photosensitizers. *Journal of Photochemistry and Photobiology B: Biology* **2014**, *138*, 1−7.
(56) Buzzá, H. H.; Zangirolami, A. C.; Davis, A.; Gómez-García, P. A.; Kurachi, C. Fluorescence analysis of a tumor model in the chorioallantoic membrane used for the evaluation of different photosensitizers for photodynamic therapy. *Photodiagnosis and Photodynamic Therapy* **2017**, *19*, 78−83.
(57) Winter, R.; Dungel, P.; Reischies, F. M. J.; Rojringer, S.; Slezak, P.; Smolle, C.; Spendel, S.; Kamolz, L.-P.; Ghaffari-Tabrizi-Wizsy, N.; Schicho, K. Photobiomodulation (PBM) promotes angiogenesis in-vitro and in chick embryo chorioallantoic membrane model. *Sci. Rep.* **2018**, *8*, 17080.
(58) Ribatti, D. The chick embryo chorioallantoic membrane (CAM). A multifaceted experimental model. *Mech. Dev.* **2016**, *141*, 70−77.
(59) Mapanao, A. K.; Che, P. P.; Sarogni, P.; Sminia, P.; Giovannetti, E.; Voliani, V. Tumor grafted - chick chorioallantoic membrane as an alternative model for biological cancer reserach and conventional/nanomaterial-based theranostics evaluation. *Expert Opinion on Drug Metabolism & Toxicology* **2021**, *17*, 947−968.
(60) Lokman, N. A.; Elder, A. S. F.; Ricciardelli, C.; Oehler, M. K. Chick Chorioallantoic Membrane (CAM) Assay as an In Vivo Model to Study the Effect of Newly Identified Molecules on Ovarian Cancer Invasion and Metastasis. *International Journal of Molecular Sciences* **2012**, *13*, 9959−9970.
(61) Becker, J.; Covelo-Fernandez, A.; von Bonin, F.; Kube, D.; Wilting, J. SPecific tumor-stroma interactions of EBV-positive Burkitt's lymphoma cells in the chick chorioallantoic membrane. *Vascular Cell* **2012**, *4*, 3.
(62) Hagedorn, M.; Javerzat, S.; Gilges, D.; Meyre, A.; de Lafarge, B.; Eichmann, A.; Bikfalvi, A. Accessing key steps of human tumor progression *in vivo* by using an avian embryo model. *Proc. Natl. Acad. Sci. U. S. A.* **2005**, *102*, 1643−1648.
(63) Fergelot, P.; Bernhard, J.-C.; Soulet, F.; Kilarski, W. W.; Léon, C.; Courtois, N.; Deminière, C.; Herbert, J. M. J.; Antczak, P.; Falciani, F.; Rioux-Leclercq, N.; Patard, J.-J.; Ferrière, J.-M.; Ravaud, A.; Hagedorn, M.; Bikfalvi, A. The experimental renal cell carcinoma model in the chick embryo. *Angiogenesis* **2013**, *16*, 181−194.
(64) Sys, G.; Van Bockstal, M.; Forsyth, R.; Balke, M.; Poffyn, B.; Uyttendaele, D.; Bracke, M.; De Wever, O. Tumor grafts derived from sarcoma patients retain tumor morphology, viability, and invasion potential and indicate disease outcomes in the chick chorioallantoic membrane model. *Cancer Letters* **2012**, *326*, 69−78.

https://doi.org/10.1021/acsnano.2c03990
ACS Nano 2022, 16, 19626−19650

(65) Kim, J.; Yu, W.; Kovalski, K.; Ossowski, L. Requirement for Specific Proteases in Cancer Cell Intravasation as Revealed by a Novel Semiquantitative PCR-Based Assay. *Cell* **1998**, *94*, 353−362.
(66) Deryugina, E. I.; Kiosses, W. B. Intratumoral Cancer Cell Intravasation Can Occur Independent of Invasion into the Adjacent Stroma. *Cell Reports* **2017**, *19*, 601−616.
(67) Schneiderhan, W.; Diaz, F.; Fundel, M.; Zhou, S.; Siech, M.; Hasel, C.; Möller, P.; Gschwend, J. E.; Seufferlein, T.; Gress, T.; Adler, G.; Bachem, M. G. Pancreatic stellate cells are an important source of MMP-2 in human pancreatic cancer and accelerate tumor progression in a murine xenograft model and CAM assay. *Journal of Cell Science* **2007**, *120*, 512−519.
(68) Chu, P.-Y.; Koh, A. P.-F.; Antony, J.; Huang, R. Y.-J. Applications of the Chick Chorioallantoic Membrane as an Alternative Model for Cancer Studies. *Cells Tissues Organs* **2022**, *211*, 222.
(69) DeBord, L. C.; Pathak, R. R.; Villaneuva, M.; Liu, H.-C.; Harrington, D. A.; Yu, W.; Lewis, M. T.; Sikora, A. G. The chick chorioallantoic membrane (CAM) as a versatile patient-derived xenograft (PDX) platform for precision medicine and preclinical research. *American Journal of Cancer Research* **2018**, *8*, 1642−1660.
(70) Lokman, N. A.; Ricciardelli, C.; Oehler, M. K., Chapter 11: Chick chorioallantoic membrane assay: a 3D animal model for cancer invasion and metastasis. *Animal Biotechnology*, Second ed.; Academic Press: New York, 2020; Vol. *1*, pp 221−231.
(71) Arpaia, E.; Blaser, H.; Quintela-Fandino, M.; Duncan, G.; Leong, H.-S.; Ablack, A.; Nambiar, S. C.; Lind, E. F.; Silvester, J.; Fleming, C. K.; Rufini, A.; Tusche, M. W.; Brüstle, A.; Ohasi, P. S.; Lewis, J. D.; Mak, T. W. The interaction between caveolin-1 and Rho-GTPases promotes metastasis by controlling the expression of alpha5-integrin and the activation of Src, Ras and Erk. *Oncogene* **2012**, *31*, 884−896.
(72) Cvetković, D.; Dragan, M.; Leith, S. J.; Mir, Z. M.; Leong, H.-S.; Pampillo, M.; Lewis, J. D.; Babwah, A. V.; Bhattacharya, M. KISS1R Induces Invasiveness of Estrogen Receptor-Negative Human Mammary Epithelial and Breast Cancer Cells. *Endocrinology* **2013**, *154*, 1999−2014.
(73) Rytelewski, M.; Buensuceso, A.; Leong, H. S.; Deroo, B. J.; Chambers, A. F.; Koropatnick, J. Evaluating the Effectiveness of Cancer Drug Sensitization *In Vitro* and *In Vivo*. *J. Visualized Exp.* **2015**, *96*, No. e52388.
(74) Rytelewski, M.; Tong, J. G.; Buensuceso, A.; Leong, H. S.; Maleki Vareki, S.; Figueredo, R.; Di Cresce, C.; Wu, S. Y.; Herbrich, S. M.; Baggerly, K. A.; Romanow, L.; Shepherd, T.; Deroo, B. J.; Sood, A. K.; Chambers, A. F.; Vincent, M.; Ferguson, P. J.; Koropatnick, J. BRCA2 inhibition enhances cisplatin-mediated alterations in tumor cell proliferation, metabolism, and metastasis. *Molecular Oncology* **2014**, *8*, 1429−1440.
(75) Sonke, E.; Verrydt, M.; Postenka, C. O.; Pardhan, S.; Willie, C. J.; Mazzola, C. R.; Hammers, M. D.; Pluth, M. D.; Lobb, I.; Power, N. E.; Chambers, A. F.; Leong, H.-S.; Sener, A. Inhibition of endogenous hydrogen sulfide production in clear-cell renal cell carcinoma cell lines and xenografts restricts their growth, survival and angiogenic potential. *Nitric Oxide* **2015**, *49*, 26−39.
(76) Kim, Y.; Williams, K. C.; Gavin, C. T.; Jardine, E.; Chambers, A. F.; Leong, H.-S. Quantification of cancer cell extravasation in vivo. *Nat. Protoc.* **2016**, *11*, 937−948.
(77) Matsumura, Y.; Maeda, H. A new concept for macromolecular therapeutics in cancer chemotherapy: mechanism of tumoritropic accumulation of proteins and the antitumor agent smancs. *Cancer Res.* **1986**, *46*, 6387−6392.
(78) Wong, A. D.; Ye, M.; Ulmschneider, M. B.; Searson, P. C. Quantitative Analysis of the Enhanced Permeation and Retention (EPR) Effect. *PLoS One* **2015**, *10*, No. e0123461.
(79) Nakamura, Y.; Mochida, A.; Choyke, P. L.; Kobayashi, H. Nanodrug Delivery: Is the Enhanced Permeability and Retention Effect Sufficient for Curing Cancer? *Bioconjugate Chem.* **2016**, *27*, 2225−2238.
(80) Liu, Y.; Huo, Y.; Yao, L.; Xu, Y.; Meng, F.; Li, H.; Sun, K.; Zhou, G.; Kohane, D. S.; Tao, K. Transcytosis of Nanomedicine for Tumor Penetration. *Nano Lett.* **2019**, *19*, 8010−8020.
(81) Pandit, S.; Dutta, D.; Nie, S. Active transcytosis and new opportunities for cancer nanomedicine. *Nat. Mater.* **2020**, *19*, 478−480.
(82) Yao, V. J.; D'Angelo, S.; Butler, K. S.; Theron, C.; Smith, T. L.; Marchio, S.; Gelovani, J. G.; Sidman, R. L.; Dobroff, A. S.; Brinker, C. J.; Bradbury, A. R.M.; Arap, W.; Pasqualini, R. Ligand-targeted theranostic nanomedicines against cancer. *J. Controlled Release* **2016**, *240*, 267−286.
(83) Vinhas, R.; Mendes, R.; Fernandes, A. R.; Baptista, P. V. Nanoparticles-emerging Potential for Managing Leukemia and Lymphoma. *Frontiers in Bioengineering and Biotechnology* **2017**, *5*, 79.
(84) Durfee, P. N.; Lin, Y.-S.; Dunphy, D. R.; Muñiz, A. J.; Butler, K. S.; Humphrey, K. R.; Lokke, A. J.; Agola, J. O.; Chou, S. S.; Chen, I.-M.; Wharton, W.; Townson, J. L.; Willman, C. L.; Brinker, C. J. Mesoporous Silica Nanoparticle-Supported Lipid Bilayers (Protocells) for Active Targeting and Delivery to Individual Leukemia Cells. *ACS Nano* **2016**, *10*, 8325−8345.
(85) Hu, C.-M. J.; Zhang, L.; Aryal, S.; Cheung, C.; Fang, R. H.; Zhang, L. Erythrocyte membrane-camouflaged polymeric nanoparticles as a biomimetic delivery platform. *Proc. Natl. Acad. Sci. U.S.A.* **2011**, *108*, 10980−10985.
(86) Townson, J. L.; Lin, Y.-S.; Agola, J. O.; Carnes, E. C.; Leong, H.-S.; Lewis, J. D.; Haynes, C. L.; Brinker, C. J. Re-examining the Size/Charge Paradigm: Differing in Vivo Characteristics of Size- and Charge-Matched Mesoporous Silica Nanoparticles. *J. Am. Chem. Soc.* **2013**, *135*, 16030−16033.
(87) Dogra, P.; Adolphi, N. L.; Wang, Z.; Lin, Y.-S.; Butler, K. S.; Durfee, P. N.; Croissant, J. G.; Noureddine, A.; Coker, E. N.; Bearer, E. L.; Cristini, V.; Brinker, C. J. Establishing the effects of mesoporous silica nanoparticle properties on in vivo disposition using imaging-based pharmacokinetics. *Nat. Commun.* **2018**, *9*, 4551.
(88) Guo, J.; Agola, J. O.; Serda, R.; Franco, S.; Lei, Q.; Wang, L.; Minster, J.; Croissant, J. G.; Butler, K. S.; Zhu, W.; Brinker, C. J. Biomimetic Rebuilding of Multifunctional Red Blood Cells: Modular Design Using Functional Components. *ACS Nano* **2020**, *14*, 7847−7859.
(89) Guo, J.; Yu, Y.; Zhu, W.; Serda, R. E.; Franco, S.; Wang, L.; Lei, Q.; Agola, J. O.; Noureddine, A.; Ploetz, E.; Wuttke, S.; Brinker, C. J. Modular Assembly of Red Blood Cell Superstructures from Metal-Organic Framework Nanoparticle-Based Building Blocks. *Adv. Funct. Mater.* **2021**, *31*, 2005935.
(90) Adlia, A.; Tomagola, I.; Damayanti, S.; Mulya, A.; Rachmawati, H. Antifibrotic Activity and In Ovo Toxicity Study of Liver-Targeted Curcumin-Gold Nanoparticle. *Scientia Pharmaceutica* **2018**, *86*, 41.
(91) Baharara, J.; Namvar, F.; Mousavi, M.; Ramezani, T.; Mohamad, R. Anti-Angiogenesis Effect of Biogenic Silver Nanoparticles Synthesized Using Saliva officinalis on Chick Chorioalantoic Membrane (CAM). *Molecules* **2014**, *19*, 13498−13508.
(92) Mroczek-Sosnowska, N.; Sawosz, E.; Vadalasetty, K. P.; Łukasiewicz, M.; Niemiec, J.; Wierzbicki, M.; Kutwin, M.; Jaworski, S.; Chwalibog, A. Nanoparticles of Copper Stimulate Angiogenesis at Systemic and Molecular Level. *International Journal of Molecular Sciences* **2015**, *16*, 4838−4859.
(93) Roth, S.; Langguth, P.; Spicher, K.; Enzmann, H. Comparative toxicity and cell-tissue distribution study on nanoparticular iron complexes using avian embryos and HepG2-cells. *Translational Research* **2008**, *151*, 36−44.
(94) Schlenk, F.; Werner, S.; Rabel, M.; Jacobs, F.; Bergemann, C.; Clement, J. H.; Fischer, D. Comprehensive analysis of the in vitro and ex ovo hemocompatibility of surface engineered iron oxide nanoparticles for biomedical applications. *Archives of toxicology* **2017**, *91*, 3271−3286.
(95) Vu, B. T.; Shahin, S. A.; Croissant, J.; Fatieiev, Y.; Matsumoto, K.; Doan, T. L.-H.; Yik, T.; Simargi, S.; Conteras, A.; Ratliff, L.; Jimenez, C. M.; Raehm, L.; Khashab, N.; Durand, J.-O.; Glackin, C.; Tamanoi, F. Chick chorioallantoic membrane assay as an in vivo

https://doi.org/10.1021/acsnano.2c03990
ACS Nano 2022, 16, 19626−19650

model to study the effect of nanoparticle-based anticancer drugs in ovarian cancer. *Sci. Rep.* **2018**, *8*, 8524.
(96) Kuzyniak, W.; Adegoke, O.; Sekhosana, K.; D'Souza, S.; Tshangana, S. C.; Hoffman, B.; Ermilov, E. A.; Nyokong, T.; Höpfner, M. Synthesis and characterization of quantum dots designed for biomedical use. *Int. J. Pharm.* **2014**, *466*, 382−389.
(97) Wierzbicki, M.; Sawosz, E.; Grodzik, M.; Prasek, M.; Jaworski, S.; Chwalibog, A. Comparison of anti-angiogenic properties of pristine carbon nanoparticles. *Nanoscale Res. Lett.* **2013**, *8*, 195.
(98) Kurantowicz, N.; Sawosz, E.; Halik, G.; Strojny, B.; Hotowy, A.; Grodzik, M.; Radoslaw, P.; Pasanphan, W.; Chwalibog, A. Toxicity studies of six types of carbon nanoparticles in a chicken-embryo model. *Int. J. Nanomed.* **2017**, *12*, 2887−2898.
(99) Peterka, M.; Klepáček, I. Light irradiation increases embryotoxicity of photodynamic therapy sensitizers (5-aminolevulinic acid and protoporphyrin IX) in chick embryos. *Reproductive Toxicology* **2001**, *15*, 111−116.
(100) Kaikabo, A. A.; Sabo Mohammed, A.; Abas, F. Chitosan Nanoparticles as Carriers for the Delivery of FKAZ14 Bacteriophage for Oral Biological Control of Colibacillosis in Chickens. *Molecules* **2016**, *21*, 256.
(101) Shkodra-Pula, B.; Grune, C.; Traeger, A.; Vollrath, A.; Schubert, S.; Fischer, D.; Schubert, U. S. Effect of surfactant on the size and stability of PLGA nanoparticles encapsulating a protein kinase C inhibitor. *Int. J. Pharm.* **2019**, *566*, 756−764.
(102) Wierzbicki, M.; Sawosz, E.; Grodzik, M.; Hotowy, A.; Prasek, M.; Jaworski, S.; Sawosz, F.; Chwalibog, A. Carbon nanoparticles downregulate expression of basic fibroblast growth factor in the heart during embryogenesis. *Int. J. Nanomed.* **2013**, *8*, 3427−3435.
(103) Samak, D. H.; El-Sayed, Y. S.; Shaheen, H. M.; El-Far, A. H.; Onoda, A.; Abdel-Daim, M. M.; Umezawa, M. In-ovo exposed carbon black nanoparticles altered mRNA gene transcripts of antioxidants, proinflammatory and apoptotic pathways in the brain of chicken embryos. *Chemico-Biological Interactions* **2018**, *295*, 133−139.
(104) Freyre-Fonseca, V.; Medina-Reyes, E. I.; Téllez-Medina, D. I.; Paniagua-Contreras, G. L.; Monroy-Pérez, E.; Vaca-Paniagua, F.; Delgado-Buenrostro, N. L.; Flores-Flores, J. O.; López-Villegas, E. O.; Gutiérrez-López, G. F.; Chirino, Y. I. Influence of shape and dispersion media of titanium dioxidenanostructures on microvessel network and ossification. *Colloids Surf., B* **2018**, *162*, 193−201.
(105) Geetha-Loganathan, P.; Nimmagadda, S.; Hafez, I.; Fu, K.; Cullis, P. R.; Richman, J. M. Development of High-Concentration Lipoplexes for In Vivo Gene Function Studies in Vertebrate Embryos. *Dev. Dyn.* **2011**, *240*, 2108−2199.
(106) Kulkarni, J. A.; Myhre, J. L.; Chen, S.; Tam, Y. Y. C.; Danescu, A.; Richman, J. M.; Cullis, P. R. Design of lipid nanoparticles for in vitro and in vivo delivery of plasmid DNA. *Nanomedicine: Nanotechnology, Biology, and Medicine* **2017**, *13*, 1377−1387.
(107) Toman, P.; Lien, C.-F.; Ahmad, Z.; Dietrich, S.; Smith, J. R.; An, Q.; Molnár, É.; Pilkington, G. J.; Górecki, D. C.; Tsibouklis, J.; Barbu, E. Nanoparticles of alkylglyceryl-dextran-graft-poly(lactic acid) for drug delivery to the brain: Preparation and in vitro investigation. *Acta Biomaterialia* **2015**, *23*, 250−262.
(108) Unterweger, H.; Dézsi, L.; Matuszak, J.; Janko, C.; Poettler, M.; Jordan, J.; Bäuerle, T.; Szebeni, J.; Fey, T.; Boccaccini, A. R.; Alexiou, C.; Cicha, I. Dextran-coated superparamagnetic iron oxide nanoparticles for magnetic resonance imaging: evaluation of size-dependent imaging properties, storage stability and safety. *Int. J. Nanomed.* **2018**, *13*, 1899−1915.
(109) Giovannini, G.; Warncke, P.; Fischer, D.; Stranik, O.; Hall, A. J.; Gubala, V. Improving colloidal stability of silica nanoparticles when stored in responsive gel: application and toxicity study. *Nanotoxicology* **2018**, *12*, 407−422.
(110) Almeida, H.; Lobão, P.; Frigerio, C.; Fonseca, J.; Silva, R.; Palmeira-de-Oliveira, A.; Lobo, J. M. S.; Amaral, M. H. New Thermoresponsive Eyedrop Formulation Containing Ibuprofen Loaded-Nanostructured Lipid Carriers (NLC): Development, Characterization and Biocompatibility Studies. *Curr. Drug Delivery* **2016**, *13*, 953−970.
(111) Eiras, F.; Amaral, M. H.; Silva, R.; Martins, E.; Sousa Lobo, J. M.; Silva, A. C. Characterization and biocompatibility evaluation of cutaneous formulations containing lipid nanoparticles. *Int. J. Pharm.* **2017**, *519*, 373−380.
(112) Passos, J. S.; de Martino, L. C.; Dartora, V. F. C.; de Araujo, G. L. B.; Ishida, K.; Lopes, L. B. Development, skin targeting and antifungal efficacy of topical lipid nanoparticles containing itraconazole. *European Journal of Pharmaceutical Sciences* **2020**, *149*, 105296.
(113) Blasi, P.; Schoubben, A.; Traina, G.; Manfroni, G.; Barberini, L.; Alberti, P. F.; Cirotto, C.; Ricci, M. Lipid nanoparticles for brain targeting III. Long-term stability and in vivo toxicity. *Int. J. Pharm.* **2013**, *454*, 316−323.
(114) Wolf, N. B.; Küchler, S.; Radowski, M. R.; Blaschke, T.; Kramer, K. D.; Weindl, G.; Kleuser, B.; Haag, R.; Schäfer-Korting, M. Influences of opioids and nanoparticles on in vitro wound healing models. *Eur. J. Pharm. Biopharm.* **2009**, *73*, 34−42.
(115) Fangueiro, J. F.; Calpena, A. C.; Clares, B.; Andreani, T.; Egea, M. A.; Veiga, F. J.; Garcia, M. L.; Silva, A. M.; Souto, E. B. Biopharmaceutical evaluation of epigallocatechin gallate-loaded cationic lipid nanoparticles (EGCG-LNs): In vivo, in vitro and ex vivo studies. *Int. J. Pharm.* **2016**, *502*, 161−169.
(116) Vasconcelos, A.; Vega, E.; Pérez, Y.; Gómara, M. J.; Garcia, M. L.; Haro, I. Conjugation of cell-penetrating peptides with poly(lactic-co-glycolic acid)-polyethylene glycol nanoparticles improves ocular drug delivery. *Int. J. Nanomed.* **2015**, *10*, 609−631.
(117) Pandit, J.; Sultana, Y.; Aqil, M. Chitosan-coated PLGA nanoparticles of bevacizumab as novel drug delivery to target retina: optimization, characterization, and in vitro toxicity evaluation. *Artificial Cells, Nanomedicine, and Biotechnology* **2017**, *45*, 1397−1407.
(118) Öztürk, A. A.; Yenilmez, E.; Şenel, B.; Kiyan, H. T.; Güven, U. M. Effect of different molecular weight PLGA on flurbiprofen nanoparticles: formulation, characterization, cytotoxicity, and in vivo antiinflammatory effect by using HET-CAM assay. *Drug Dev. Ind. Pharm.* **2020**, *46*, 682−695.
(119) Flores, F. C.; Rosso, R. S.; Cruz, L.; Beck, R. C. R.; Silva, C. B. An innovative polysaccharide nanobased nail formulation for improvement of onychomycosis treatment. *European Journal of Pharmaceutical Sciences* **2017**, *100*, 56−63.
(120) Katzer, T.; Chaves, P.; Bernardi, A.; Pohlmann, A. R.; Guterres, S. S.; Beck, R. C. R. Prednisolone-loaded nanocapsules as ocular drug delivery system: development, in vitro drug release and eye toxicity. *J. Microencapsulation* **2014**, *31*, 519−528.
(121) Álvarez-Álvarez, L.; Barral, L.; Bouza, R.; Farrag, Y.; Otero-Espinar, F.; Feijóo-Bandín, S.; Lago, F. Hydrocortisone loaded poly-(3-hydroxybutyrate-co-3-hydroxyvalerate) nanoparticles for topical ophthalmic administration: Preparation, characterization and evaluation of ophthalmic toxicity. *Int. J. Pharm.* **2019**, *568*, 118519.
(122) Bakan, B.; Gülcemal, S.; Akgöl, S.; Hoet, P. H. M.; Yavapoḍlu, N. U. K. Synthesis, characterization and toxicity assessment of a new polymeric nanoparticle, L-glutamic acid-g-p(HEMA). *Chemico-Biological Interactions* **2020**, *315*, 108870.
(123) Pathak, D.; Kumar, P.; Kuppusamy, G.; Gupta, A.; Kamble, B.; Wadhwani, A. Physicochemical characterization and toxicological evaluation of plantbased anionic polymers and their nanoparticulated system for ocular delivery. *Nanotoxicology* **2014**, *8*, 843−855.
(124) Katzer, T.; Chaves, P.; Bernardi, A.; Pohlmann, A. R.; Guterres, S. S.; Beck, R. C. R. Castor oil and mineral oil nanoemulsion: development and compatibility with a soft contact lens. *Pharm. Dev. Technol.* **2014**, *19*, 232−237.
(125) Ambhore, N. P.; Dandagi, P. M.; Gadad, A. P. Formulation and comparative evaluation of HPMC and water soluble chitosan-based sparfloxacin nanosuspension for ophthalmic delivery. *Drug Delivery and Translational Research* **2016**, *6*, 48−56.
(126) Dilbaghi, N.; Kaur, H.; Ahuja, M.; Kumar, S. Evaluation of tropicamide-loaded tamarind seed xyloglucan nanoaggregates for ophthalmic delivery. *Carbohydr. Polym.* **2013**, *94*, 286−291.
(127) Cirik, S.; Elesad, M.; Başar, E.; Aksu, E.; Erdem, M.; Yildiztekîn, F.; Menekşe, S.; Çelîkel, R.; İpek, M. Y.; Fermanli, O.; Eşrefoğlu, M. Effects of Gold Nanoparticles on Angiogenesis in A

https://doi.org/10.1021/acsnano.2c03990
ACS Nano 2022, 16, 19626−19650

Chick Chorioallantoic Membrane Model. *Bezmialem Science* **2020**, *8*, 398−402.
(128) Pan, Y.; Wu, Q.; Qin, L.; Cai, J.; Du, B. Gold Nanoparticles Inhibit VEGF165-Induced Migration and Tube Formation of Endothelial Cells via the Akt Pathway. *BioMed. Research International* **2014**, *2014*, 418624.
(129) Vimalraj, S.; Ashokkumar, T.; Saravanan, S. Biogenic gold nanoparticles synthesis mediated by Mangifera indica seed aqueous extracts exhibits antibacterial, anticancer and anti-angiogenic properties. *Biomedicine & Pharmacotherapy* **2018**, *105*, 440−448.
(130) Pedrosa, P.; Heuer-Jungemann, A.; Kanaras, A. G.; Fernandez, A. R.; Baptista, P. V. Potentiating angiogenesis arrest in vivo via laser irradiation of peptide functionalised gold nanoparticles. *J. Nanobiotechnol.* **2017**, *15*, 85.
(131) Roma-Rodrigues, C.; Fernandes, A. R.; Baptista, P. V. Counteracting the effect of leukemia exosomes by antiangiogenic gold nanoparticles. *Int. J. Nanomed.* **2019**, *14*, 6843−6854.
(132) Roma-Rodrigues, C.; Heuer-Jungemann, A.; Fernandes, A. R.; Kanaras, A. G.; Baptista, P. V. Peptide-coated gold nanoparticles for modulation of angiogenesis in vivo. *Int. J. Nanomed.* **2016**, *11*, 2633−2639.
(133) Rajan, A.; Praseetha, P. K.; Ariharan, V. N.; Gopu Kumar, S. T. In-vitro Chick Chorioallantoic Membrane Study of Chitosan Capped 5-Fluorouracil Conjugated Gold Nanoparticles. *Journal of Pharmaceutical Sciences and Research* **2019**, *11*, 2090−2094.
(134) Harmankaya, O. F.; Hamsho, A.; Goztepe, M.; Baghirova, S.; Cirik, S.; Sirin, H.; Alasad, M.; Sari, B. S.; Uckun, I.; Kocer, A.; Aksu, E.; Farmanli, O. The Effect of Chitosan Capped Copper Nanoparticles on Angiogenesis in Cam Assay. *Biomedical Journal of Science & Technical Research* **2021**, *35*, 27971.
(135) Rahimi Kalateh Shah Mohammad, G.; Homayouni Tabrizi, M.; Ardalan, T.; Yadamani, S.; Safavi, E. Green synthesis of zinc oxide nanoparticles and evaluationof anti-angiogenesis, anti-inflammatory and cytotoxicityproperties. *Journal of biosciences* **2019**, *44*, 30.
(136) Divya, M.; Vaseeharan, B.; Abinaya, M.; Vijayakumar, S.; Govindarajan, M.; Alharbi, N. S.; Kadaikunnan, S.; Khaled, J. M.; Benelli, G. Biopolymer gelatin-coated zinc oxide nanoparticles showed high antibacterial, antibiofilm and anti-angiogenic activity. *Journal of Photochemistry and Photobiology B: Biology* **2018**, *178*, 211−218.
(137) Sanaeimehr, Z.; Javadi, I.; Namvar, F. Antiangiogenic and antiapoptotic effects of green.synthesized zinc oxide nanoparticles using Sargassum muticum algae extraction. *Cancer Nanotechnology* **2018**, *9*, 3.
(138) Muchová, J.; Hearnden, V.; Michlovská, L.; Vištejnová, L.; Zavaďáková, A.; Šmerková, K.; Kočiová, S.; Adam, V.; Kopel, P.; Vojtová, L. Mutual influence of selenium nanoparticles and FGF2-STAB® on biocompatible properties of collagen/chitosan 3D scaffolds: in vitro and ex ovo evaluation. *J. Nanobiotechnol.* **2021**, *19*, 103.
(139) Augustine, R.; Dalvi, Y. B.; Yadu Nath, V.K.; Varghese, R.; Raghuveeran, V.; Hasan, A.; Thomas, S.; Sandhyarani, N. Yttrium oxide nanoparticle loaded scaffolds with enhanced cell adhesion and vascularization for tissue engineering applications. *Mater. Sci. Eng., C* **2019**, *103*, 109801.
(140) Hu, H.; You, Y.; He, L.; Chen, T. The rational design of NAMI-A-loaded mesoporous silica nanoparticles as antiangiogenic nanosystems. *J. Mater. Chem. B* **2015**, *3*, 6338−6346.
(141) Kim, J.-H.; Kim, T.-H.; Kang, M. S.; Kim, H.-W. Angiogenic Effects of Collagen/Mesoporous Nanoparticle Composite Scaffold Delivering VEGF165. *BioMed. Research International* **2016**, *2016*, 9676934.
(142) Nooris, M.; Aparna, D.; Radha, S. Synthesis and characterization of MFe2O4 (M = Co, Ni, Mn) magnetic nanoparticles formodulation ofangiogenesis inchick chorioallantoic membrane (CAM). *Eur. Biophys. J.* **2016**, *45*, 139−148.
(143) Shereema, R. M.; Sruthi, T. V.; Sameer Kumar, V. B.; Rao, T. P.; Sharath Shankar, S. Angiogenic Profiling of Synthesized Carbon Quantum Dots. *Biochemistry* **2015**, *54*, 6352−6356.
(144) Murugesan, S.; Mousa, S. A.; O'Connor, L.; Lincoln II, D. W.; Lindhardt, R. J. Carbon inhibits vascular endothelial growth factor- and fibroblast growth factor-promoted angiogenesis. *FEBS Lett.* **2007**, *581*, 1157−1160.
(145) Bharti, R.; Dey, G.; Banerjee, I.; Dey, K. K.; Parida, S.; Kumar, B. N. P.; Das, C. K.; Pal, I.; Mukherjee, M.; Misra, M.; Pradhan, A. K.; Emdad, L.; Das, S. K.; Fisher, P. B.; Mandal, M. Somatostatin receptor targeted liposomes with Diacerein inhibit IL-6 for breast cancer therapy. *Cancer Letters* **2017**, *388*, 292−302.
(146) Guo, P.; Yang, J.; Jia, D.; Moses, M. A.; Auguste, D. T. ICAM-1-Targeted, Lcn2 siRNA-Encapsulating Liposomes are Potent Anti-angiogenic Agents for Triple Negative Breast Cancer. *Theranostics* **2016**, *6*, 1−13.
(147) Mandracchia, D.; Tripodo, G.; Trapani, A.; Ruggieri, S.; Annese, T.; Chalpanidas, T.; Trapani, G.; Ribatti, D. Inulin based micelles loaded with curcumin or celecoxib with effective anti-angiogenic activity. *European Journal of Pharmaceutical Sciences* **2016**, *93*, 141−146.
(148) Krishnaswami, V.; Ponnusamy, C.; Sankareswaran, S.; Paulsamy, M.; Madiyalakan, R.; Palanichamy, R.; Kandasamy, R.; Natesan, S. Development of copolymeric nanoparticles of hypocrellin B: Enhanced phototoxic effect and ocular distribution. *European Journal of Pharmaceutical Sciences* **2018**, *116*, 26−36.
(149) Zhao, Y.; Xiao, W.; Peng, W.; Huang, Q.; Wu, K.; Evans, C. E.; Liu, X.; Jin, H. Oridonin-Loaded Nanoparticles Inhibit Breast Cancer Progression Through Regulation of ROS-Related Nrf2 Signaling Pathway. *Frontiers in Bioengineering and Biotechnology* **2021**, *9*, 600579.
(150) Dias, M. F.; de Figueiredo, B. C. P.; Teixeira-Neto, J.; Guerra, M. C. A.; Fialho, S. L.; Cunha, A. S. In vivo evaluation of antitumoral and antiangiogenic effect of imiquimod-loaded polymeric nanoparticles. *Biomedicine & Pharmacotherapy* **2018**, *103*, 1107−1114.
(151) Mansur, A. A. P.; Carvalho, S. M.; Lobato, Z. I. P.; de Faìtima Leite, M.; da Silva Cunha Júnior, A.; Mansur, H. S. Design and Development of Polysaccharide-Doxorubicin-Peptide Bioconjugates for Dual Synergistic Effects of Integrin-Targeted and Cell-Penetrating Peptides for Cancer Chemotherapy. *Bioconjugate Chem.* **2018**, *29*, 1973−2000.
(152) Yang, F.; Fang, X.; Jiang, W.; Chen, T. Bioresponsive cancer-targeted polysaccharide nanosystem to inhibit angiogenesis. *Int. J. Nanomed.* **2017**, *12*, 7419−7431.
(153) Ferreira, L. M. B.; Alonso, J. D.; Kiill, C. P.; Ferreira, N. N.; Buzzá, H. H.; Martins de Godoi, D. R.; de Britto, D.; Assis, O. B. G.; Seraphim, T. V.; Borges, J. C.; Gremião, M. P. D. Exploiting supramolecular interactions to produce bevacizumab-loaded nanoparticles for potential mucosal delivery. *Eur. Polym. J.* **2018**, *103*, 238−250.
(154) Jin, H.; Pi, J.; Yang, F.; Wu, C.; Cheng, X.; Bai, H.; Huang, D.; Jiang, J.; Cai, J.; Chen, Z. W. Ursolic acid-loaded chitosan nanoparticles induce potent anti-angiogenesis in tumor. *Appl. Microbiol. Biotechnol.* **2016**, *100*, 6643−6652.
(155) Jain, K.; Gupta, U.; Jain, N. K. Dendronized nanoconjugates of lysine and folate for treatment of cancer. *Eur. J. Pharm. Biopharm.* **2014**, *87*, 500−509.
(156) Jain, K.; Jain, N. K. Surface Engineered Dendrimers as Antiangiogenic Agent and Carrier for Anticancer Drug: Dual Attack on Cancer. *J. Nanosci. Nanotechnol.* **2014**, *14*, 5075−5087.
(157) Al-Jamal, K.; Al-Jamal, W. T.; Akerman, S.; Podesta, J. E.; Yilmazer, A.; Turton, J. A.; Bianco, A.; Vargesson, N.; Kanthou, C.; Florence, A. T.; Tozer, G. M.; Kostarelos, K. Systemic antiangiogenic activity of cationic poly-L-lysine dendrimer delays tumor growth. *Proc. Natl. Acad. Sci. U.S.A.* **2010**, *107*, 3966−3971.
(158) Dehelean, C. A.; Feflea, S.; Gheorgheosu, D.; Ganta, S.; Cimpean, A. M.; Muntean, D.; Amiji, M. M. Anti-Angiogenic and Anti-Cancer Evaluation of Betulin Nanoemulsion in Chicken Chorioallantoic Membrane and Skin Carcinoma in Balb/c Mice. *Journal of Biomedical Nanotechnology* **2013**, *9*, 577−589.
(159) Pund, S.; Borade, G.; Rasve, G. Improvement of anti-inflammatory and anti-angiogenic activity of berberine by novel rapid

https://doi.org/10.1021/acsnano.2c03990
ACS Nano 2022, 16, 19626−19650

dissolving nanoemulsifying technique. *Phytomedicine* **2014**, *21*, 307−314.
(160) Pund, S.; Thakur, R.; More, U.; Joshi, A. Lipid based nanoemulsifying resveratrol for improved physicochemical characteristics, in vitro cytotoxicity and in vivo antiangiogenic efficacy. *Colloids Surf., B* **2014**, *120*, 110−117.
(161) Maia, A. L. C.; de Aguiar Ferreira, C.; de Barros, A. L. B.; Maciel e Silva, A. T.; Ramaldes, G. A.; da Silva Cunha Júnior, A.; de Pádua Oliveira, D. C.; Fernandes, C.; Soares, D. C. F. Vincristine-loaded hydroxyapatite nanoparticles as a potential delivery system for bone cancer therapy. *J. Drug Targeting* **2018**, *26*, 592−603.
(162) Garrier, J.; Reshetov, V.; Gräfe, S.; Guillemin, F.; Zorin, V.; Bezdetnaya, L. Factors affecting the selectivity of nanoparticle-based photoinduced damage in free and xenografted chorioallantoic membrane model. *J. Drug Targeting* **2014**, *22*, 220−231.
(163) Pegaz, B.; Debefve, E.; Ballini, J.-P.; Wagnières, G.; Spaniol, S.; Albrecht, V.; Scheglmann, D. V.; Nifantiev, N. E.; van den Bergh, H.; Konan-Kouakou, Y. N. Photothrombic activity of m-THPC-loaded liposomal formulations: Pre-clinical assessment on chick chorioallantoic membrane model. *European Journal of Pharmaceutical Sciences* **2006**, *28*, 134−140.
(164) Gottfried, V.; Davidi, R.; Averbuj, C.; Kimel, S. In vivo damage to chorioallantoic membrane blood vessels by porphycene-induced photodynamic therapy. *Journal of Photochemistry and Photobiology B: Biology* **1995**, *30*, 115−121.
(165) Toledano, H.; Edrei, R.; Kimel, S. Photodynamic damage by liposome-bound porphycenes: comparison between in vitro and in vivo models. *Journal of Photochemistry and Photobiology B: Biology* **1998**, *42*, 20−27.
(166) Hammer-Wilson, M. J.; Akian, L.; Espinoza, J.; Kimel, S.; Berns, M. W. Photodynamic parameters in the chick chorioallantoic membrane (CAM) bioassay for topically applied photosensitizers. *Journal of Photochemistry and Photobiology B: Biology* **1999**, *53*, 44−52.
(167) Hammer-Wilson, M. J.; Cao, D.; Kimel, S.; Berns, M. W. Photodynamic parameters in the chick chorioallantoic membrane (CAM) bioassay for photosensitizers administered intraperitoneally (IP) into the chick embryo. *Photochemical and Photobiological Sciences* **2002**, *1*, 721−728.
(168) Hornung, R.; Hammer-Wilson, M. J.; Kimel, S.; Liaw, L.-H.; Tadir, Y.; Berns, M. W. Systemic application of photosensitizers in the chick chorioallantoic membrane (CAM) model: photodynamic response of CAM vessels and 5-aminolevulinic acid uptake kinetics by transplantable tumors. *Journal of Photochemistry and Photobiology B: Biology* **1999**, *49*, 41−49.
(169) Lange, N.; Ballini, J.-P.; Wagnières, G.; Van den Bergh, H. A New Drug-Screening Procedure for Photosensitizing Agents Used in Photodynamic Therapy for CNV. *Investigative Ophthalmology & Visual Science* **2001**, *42*, 38−46.
(170) Pegaz, B.; Debefve, E.; Ballini, J.-P.; Konan-Kouakou, Y. N.; van den Bergh, H. Effect of nanoparticle size on the extravasation and the photothrombic activity of meso(p-tetracarboxyphenyl)porphyrin. *Journal of Photochemistry and Photobiology B: Biology* **2006**, *85*, 216−222.
(171) Pegaz, B.; Debefve, E.; Borle, F.; Ballini, J.-P.; van den Bergh, H.; Kouakou-Konan, Y. N. Encapsulation of porphyrins and chlorins in biodegradable nanoparticles: The effect of dye lipophilicity on the extravasation and the photothrombic activity. A comparative study. *Journal of Photochemistry and Photobiology B: Biology* **2005**, *80*, 19−27.
(172) Vargas, A.; Pegaz, B.; Debefve, E.; Konan-Kouakou, Y. N.; Lange, N.; Ballini, J.-P.; van den Bergh, H.; Gurny, R.; Delie, F. Improved photodynamic activity of porphyrin loaded into nanoparticles: an in vivo evaluation using chick embryos. *Int. J. Pharm.* **2004**, *286*, 131−145.
(173) Niemelä, E.; Desai, D.; Niemi, R.; Doroszko, M.; Özliseli, E.; Kemppainen, K.; Rahman, N. A.; Sahlgren, C.; Törnquist, K.; Eriksson, J. E.; Rosenholm, J. M. Nanoparticles carrying fingolimod and methotrexate enables targeted induction of apoptosis and immobilization of invasive thyroid cancer. *Eur. J. Pharm. Biopharm.* **2020**, *148*, 1−9.
(174) Paris, J. L.; Villaverde, G.; Gómez-Graña, S.; Vallet-Regí, M. Nanoparticles for multimodal antivascular therapeutics: Dual drug release, photothermal and photodynamic therapy. *Acta Biomaterialia* **2020**, *101*, 459−468.
(175) Liu, L.-Z.; Ding, M.; Zheng, J. Z.; Zhu, Y.; Fenderson, B. A.; Li, B.; Yu, J. J.; Jiang, B.-H. Tungsten Carbide-Cobalt Nanoparticles Induce Reactive Oxygen Species, AKT, ERK, AP-1, NF-κB, VEGF, and Angiogenesis. *Biological Trace Element Research* **2015**, *166*, 57−65.
(176) Ismail, M. S.; Torsten, U.; Dressler, C.; Diederichs, J. E.; Hüske, S.; Weitzel, H.; Berlien, H.-P. Photodynamic Therapy of Malignant Ovarian Tumours Cultivated on CAM. *Lasers in Medical Science* **1999**, *14*, 91−96.
(177) Pastorino, F.; Brignole, C.; Di Paolo, D.; Nico, B.; Pezzolo, A.; Marimpietri, D.; Pagnan, G.; Piccardi, F.; Cilli, M.; Longhi, R.; Ribatti, D.; Corti, A.; Allen, T. M.; Ponzoni, M. Targeting Liposomal Chemotherapy via Both Tumor Cell-Specific and Tumor Vasculature-Specific Ligands Potentiates Therapeutic Efficacy. *Cancer Res.* **2006**, *66*, 10073−10082.
(178) Pastorino, F.; di Paolo, D.; Piccardi, F.; Nico, B.; Ribatti, D.; Daga, A.; Baio, G.; Neumaier, C. E.; Brignole, C.; Loi, M.; Marimpietri, D.; Pagnan, G.; Cilli, M.; Lepekhin, E. A.; Garde, S. V.; Longhi, R.; Corti, A.; Allen, T. M.; Wu, J. J.; Ponzoni, M. Enhanced Antitumor Efficacy of Clinical-GradeVasculature-Targeted Liposomal Doxorubicin. *Clin. Cancer Res.* **2008**, *14*, 7320−7329.
(179) Mousa, S. A.; Yalcin, M.; Bharali, D. J.; Meng, R.; Tang, H.-Y.; Lin, H.-Y.; Davis, F. B.; Davis, P. J. Tetraiodothyroacetic acid and its nanoformulation inhibit thyroid hormone stimulation of non-small cell lung cancer cells in vitro and its growth in xenografts. *Lung Cancer* **2012**, *76*, 39−45.
(180) Yalcin, M.; Bharali, D. J.; Dyskin, E.; Dier, E.; Lansing, L.; Mousa, S. S.; Davis, F. B.; Davis, P. J.; Mousa, S. A. Tetraiodothyroacetic Acid and Tetraiodothyroacetic Acid Nanoparticle Effectively Inhibit the Growth of Human Follicular Thyroid Cell Carcinoma. *Thyroid* **2010**, *20*, 281−286.
(181) Yalcin, M.; Bharali, D. J.; Lansing, L.; Dyskin, E.; Mousa, S. S.; Hercbergs, A.; Davis, F. B.; Davis, P. J.; Mousa, S. A. Tetraiodothyroacetic Acid (Tetrac) and Tetrac Nanoparticles Inhibit Growth of Human Renal Cell Carcinoma Xenografts. *Anticancer Res.* **2009**, *29*, 3825−3832.
(182) Cho, C.-F.; Yu, L.; Nsiama, T. K.; Kadam, A. N.; Raturi, A.; Shukla, S.; Amadei, G. A.; Steinmetz, N. F.; Luyt, L. G.; Lewis, J. D. Viral nanoparticles decorated with novel EGFL7 ligands enable intravital imaging of tumor neovasculature. *Nanoscale* **2017**, *9*, 12096.
(183) Cho, C.-F.; Ablack, A.; Leong, H.-S.; Zijlstra, A.; Lewis, J. Evaluation of Nanoparticle Uptake in Tumors in Real Time Using Intravital Imaging. *J. Visualized Exp.* **2011**, *52*, No. e2808.
(184) Steinmetz, N. F.; Cho, C.-F.; Ablack, A.; Lewis, J. D.; Manchester, M. Cowpea mosaic virus nanoparticles target surface vimentin on cancer cells. *Nanomedicine (London)* **2011**, *6*, 351−364.
(185) Lee, G. S.; Filipovic, N.; Miele, L. F.; Lin, M.; Simpson, D. C.; Giney, B.; Konerding, M. A.; Tsuda, A.; Mentzer, S. J. Blood flow shapes intravascular pillar geometry inthe chick chorioallantoic membrane. *Journal of Angiogenesis Research* **2010**, *2*, 11.
(186) Liu, Z. L.; Clausen, J. R.; Wagner, J. L.; Butler, K. S.; Bolintineanu, D. S.; Lechman, J. B.; Rao, R. R.; Aidun, C. K. Heterogeneous partition of cellular blood-borne nanoparticles through microvascular bifurcations. *Phys. Rev. E* **2020**, *102*, 013310.
(187) Clancy, A. A.; Gregoriou, Y.; Yaehne, K.; Cramb, D. Measuring properties of nanoparticles in embryonic blood vessels: Towards a physicochemical basis for nanotoxicity. *Chem. Phys. Lett.* **2010**, *488*, 99−111.
(188) Müller, R.; Stranik, O.; Schlenk, F.; Werner, S.; Malsch, D.; Fischer, D.; Fritzsche, W. Optical detection of nanoparticle agglomeration in a living system under the influence of a magnetic field. *J. Magn. Magn. Mater.* **2015**, *380*, 61−65.
(189) Palmer, T. D.; Lewis, J.; Zijlstra, A. Quantitative Analysis of Cancer Metastasis using an Avian Embryo Model. *J. Visualized Exp.* **2011**, *51*, No. e2815.

https://doi.org/10.1021/acsnano.2c03990
ACS Nano 2022, 16, 19626−19650

(190) Xiao, X.; Zhou, X.; Ming, H.; Zhang, J.; Huang, G.; Zhang, Z.; Li, P. Chick Chorioallantoic Membrane Assay: A 3D Animal Model for Study of Human Nasopharyngeal Carcinoma. *PLoS One* **2015**, *10*, No. e0130935.
(191) Leong, H.-S.; Lizardo, M. M.; Ablack, A.; McPherson, V. A.; Wandless, T. J.; Chambers, A. F.; Lewis, J. D. Imaging the Impact of Chemically Inducible Proteins on Cellular Dynamics In Vivo. *PLoS One* **2012**, *7*, No. e30177.
(192) Croissant, J. G.; Butler, K. S.; Zink, J. I.; Brinker, C. J. Synthetic amorphous silica nanoparticles: toxicity, biomedical and environmental implications. *Nature Reviews Materials* **2020**, *5*, 886−909.
(193) Ademi, H.; Shinde, D. A.; Gassmann, M.; Gerst, D.; Chaachouay, H.; Vogel, J.; Gorr, T. A. Targeting neovascularization and respiration of tumor grafts grown on chick embryo chorioallantoic membranes. *PLoS One* **2021**, *16*, No. e0251765.
(194) Eckrich, J.; Kugler, P.; Buhr, C. R.; Ernst, B. P.; Mendler, S.; Baumgart, J.; Brieger, J.; Wiesmann, N. Monitoring of tumor growth and vascularization with repetitive ultrasonography in the chicken chorioallantoic-membrane-assay. *Sci. Rep.* **2020**, *10*, 18585.
(195) Huang, C.; Lowerison, M. R.; Lucien, F.; Gong, P.; Wnag, D.; SOng, P.; Chen, S. Noninvasive Contrast-Free 3D Evaluation of Tumor Angiogenesis with Ultrasensitive Ultrasound Microvessel Imaging. *Sci. Rep.* **2019**, *9*, 4907.
(196) Canavese, G.; Ancona, A.; Racca, L.; Canta, M.; Dumontel, B.; Barbaresco, F.; Limongi, T.; Cauda, V. Nanoparticle-assisted ultrasound: A special focus on sonodynamic therapy against cancer. *Chemical Engineering Journal* **2018**, *340*, 155−172.
(197) Tharkar, P.; Varanasi, R.; Wong, W. S. F.; Jin, C. T.; Chrzanowski, W. Nano-Enhanced Drug Delivery and Therapeutic Ultrasound for Cancer Treatment and Beyond. *Frontiers in Bioengineering and Biotechnology* **2019**, *7*, 324.
(198) Li, L.; Guan, Y.; Xiong, H.; Deng, T.; Ji, Q.; Xu, Z.; Kang, Y.; Pang, J. Fundamentals and applications of nanoparticles for ultrasound-based imaging and therapy. *Nano Select* **2020**, *1*, 263−284.
(199) Winter, G.; Koch, A. B. F.; Löffler, J.; Jelezko, F.; Lindén, M.; Li, H.; Abaei, A.; Beer, A. J.; Rasche, V. In vivo PET/MRI Imaging of the Chorioallantoic Membrane. *Frontiers in Physics* **2020**, *8*, 151.
(200) Lindner, T.; Klose, R.; Streckenbach, F.; Stahnke, T.; Hadlich, S.; Kuhn, J.-P.; Guthoff, R. F.; Wree, A.; Neumann, A.-M.; Frank, M.; Glass, A.; Langner, S.; Stachs, O. Morphologic and biometric evaluation of chick embryo eyes in ovo using 7 T MRI. *Sci. Rep.* **2017**, *7*, 2647.
(201) Zhou, Z.; Chen, Z.; Shan, J.; Ma, W.; Zu, J.; Xu, J. Monitoring brain development of chick embryos in vivo using 3.0 T MRI: subdivision volume change and preliminary structural quantification using DTI. *BMC Developmental Biology* **2015**, *15*, 29.
(202) Zuo, Z.; Syrovets, T.; Wu, Y.; Hafner, S.; Vernikouskaya, I.; Liu, W.; Ma, G.; Weil, T.; Simmet, T.; Rasche, V. The CAM cancer xenograft as a model for initial evaluation of MR labelled compounds. *Sci. Rep.* **2017**, *7*, 46690.
(203) Hafner, S.; Raabe, M.; Wu, Y.; Wang, T.; Zuo, Z.; Rasche, V.; Syrovets, T.; Weil, T.; Simmet, T. High-Contrast Magnetic Resonance Imaging and Efficient Delivery of an Albumin Nanotheranostic in Triple-Negative Breast Cancer Xenografts. *Advanced Therapeutics* **2019**, *2*, 1900084.
(204) Oppitz, M.; Pintaske, J.; Kehlbach, R.; Schick, F.; Schriek, G.; Busch, C. Magnetic resonance imaging of iron-oxide labeled SK-Mel 28 human melanoma cells in the chick embryo using a clinical whole body MRI scanner. *Magnetic Resonance Materials in Physics Biology and Medicine* **2007**, *20*, 1−9.
(205) Taylor, A.; Herrmann, A.; Moss, D.; Sée, V.; Davies, K.; Williams, S. R.; Murray, P. Assessing the Efficacy of Nano- and Micro-Sized Magnetic Particles as Contrast Agents for MRI Cell Tracking. *PLoS One* **2014**, *9*, No. e100259.
(206) Faucher, L.; Guay-Begin, A.-A.; Lagueux, J.; Cote, M.-F.; Petitclerc, E.; Fortin, M.-A. Ultra-small gadolinium oxide nanoparticles to image brain cancer cells in vivo with MRI. *Contrast Media & Molecular Imaging* **2010**, *6*, 209−218.
(207) Haller, S.; Ametamey, S. M.; Schibli, R.; Müller, C. Investigation of the chick embryo as a potential alternative to the mouse for evaluation of radiopharmaceuticals. *Nuclear Medicine and Biology* **2015**, *42*, 226−233.
(208) Warnock, G.; Turtoi, A.; Bloome, A.; Bretin, F.; Bahri, M. A.; Lemaire, C.; Libert, L. C.; Seret, A. E. J. J.; Luxen, A.; Castronovo, V.; Plenevaux, A. R. E. G. In Vivo PET/CT in a Human Glioblastoma Chicken Chorioallantoic Membrane Model: A New Tool for Oncology and Radiotracer Development. *Journal of Nuclear Medicine* **2013**, *54*, 1782−1788.
(209) The Roslin Institute National Avian Research Facility Genetically altered lines. https://www.ed.ac.uk/roslin/national-avian-research-facility/avian-resources/genetically-altered-lines (accessed 3/16/2022).
(210) McGrew, M. J.; Sherman, A.; Lillico, S. G.; Ellard, F. M.; Radcliffe, P. A.; Gilhooley, H. J.; Mitrophanous, K. A.; Cambray, N.; Wilson, V.; Sang, H. Localised axial progenitor cell populations in the avian tail bud are not committed to a posterior Hox identity. *Development* **2008**, *135*, 2289−2299.
(211) Ho, W. K. W.; Freem, L.; Zhao, D.; Painter, K. J.; Woolley, T. E.; Gaffney, E. A.; McGrew, M. J.; Tzika, A.; Milinkovitch, M. C.; Schneider, P.; Drusko, A.; Matthäus, F.; Glover, J. D.; Wells, K. L.; Johansson, J. A.; Davey, M. G.; Sang, H. M.; Clinton, M.; Headon, D. J. Feather arrays are patterned by interacting signalling and cell density waves. *PLoS Biology* **2019**, *17*, No. e3000132.
(212) Garceau, V.; Balic, A.; Garcia-Morales, C.; Sauter, K. A.; McGrew, M. J.; Smith, J.; Vervelde, L.; Sherman, A.; Fuller, T. E.; Oliphant, T.; Shelley, J. A.; Tiwari, R.; Wilson, T. L.; Chintoan-Uta, C.; Burt, D. W.; Stevens, M. P.; Sang, H. M.; Hume, D. A. The development and maintenance of the mononuclear phagocyte system of the chick is controlled by signals from the macrophage colony-stimulating factor receptor. *BMC Biology* **2015**, *13*, 12.
(213) Ballantyne, M.; Woodcock, M.; Doddamani, D.; Hu, T.; Taylor, L.; Hawken, R. J.; McGrew, M. J. Direct allele introgression into pure chicken breeds using Sire Dam Surrogate (SDS) mating. *Nat. Commun.* **2021**, *12*, 659.
(214) Taylor, L.; Carlson, D. F.; Nandi, S.; Sherman, A.; Fahrenkrug, S. C.; McGrew, M. J. Efficient TALEN-mediated gene targeting of chicken primordial germ cells. *Development* **2017**, *144*, 928−934.
(215) Soulet, F.; Kilarski, W. W.; Roux-Dalvai, F.; Herbert, J. M. J.; Sacewicz, I.; Mouton-Barbosa, E.; Bicknell, R.; Lalor, P.; Monsarrat, B.; Bikfalvi, A. Mapping the Extracellular and Membrane Proteome Associated with the Vasculature and the Stroma in the Embryo. *Molecular & Cellular Proteomics* **2013**, *12*, 2293−2312.
(216) Walkey, C. D.; Chan, W. C. W. Understanding and controlling the interaction of nanomaterials with proteins in a physiological environment. *Chem. Soc. Rev.* **2012**, *41*, 2780−2799.
(217) Tenzer, S.; Docter, D.; Kauharev, J.; Musyanovych, A.; Fetz, V.; Hecht, R.; Schlenk, F.; Fischer, D.; Kiouptsi, K.; Reinhardt, C.; Landfester, K.; Schild, H.; Maskos, M.; Knauer, S. K.; Stauber, R. H. Rapid formation of plasma protein corona critically affects nanoparticle pathophysiology. *Nat. Nanotechnol.* **2013**, *8*, 772−781.
(218) Patel, S.; Jana, S.; Chetty, R.; Thakore, S.; Singh, M.; Devkar, R. TiO_2 nanoparticles induce omphalocele in chicken embryo by disrupting Wnt signaling pathway. *Sci. Rep.* **2018**, *8*, 4756.
(219) Balan, P.; Indrakumar, J.; Murali, P.; Korrapati, P. S. Bi-faceted delivery of phytochemicals through chitosan nanoparticles impregnated nanofibers for cancer therapeutics. *Int. J. Biol. Macromol.* **2020**, *142*, 201−211.
(220) Tang, Y.; Cai, R.; Cao, D.; Kong, X.; Lu, Y. Photocatalytic production of hydroxyl radicals by commercial TiO2 nanoparticles and phototoxic hazard identification. *Toxicology* **2018**, *406*−*407*, 1−8.
(221) Vargas, A.; Eid, M.; Fanchaouy, M.; Gurny, R.; Delie, F. In vivo photodynamic activity of photosensitizer-loaded nanoparticles: Formulation properties, administration parameters and biological issues involved in PDT outcome. *Eur. J. Pharm. Biopharm.* **2008**, *69*, 43−53.
(222) Wierzbicki, M.; Jaworski, S.; Sawosz, E.; Jung, A.; Gielerak, G.; Jaremek, H.; Łojkowski, W.; Wozniak, B.; Stobinski, L.; Małolepszy,

https://doi.org/10.1021/acsnano.2c03990
ACS Nano 2022, 16, 19626−19650

A.; Chwalibog, A. Graphene Oxide in a Composite with Silver Nanoparticles Reduces the Fibroblast and Endothelial Cell Cytotoxicity of an Antibacterial Nanoplatform. *Nanoscale Res. Lett.* **2019**, *14*, 320.
(223) Tariq, I.; Pinnapireddy, S. R.; Duse, L.; Ali, M. Y.; Ali, S.; Amin, M. U.; Goergen, N.; Jedelská, J.; Schäfer, J.; Bakowsky, U. Lipodendriplexes: A promising nanocarrier for enhanced gene delivery with minimal cytotoxicity. *Eur. J. Pharm. Biopharm.* **2019**, *135*, 72−82.
(224) Kingston, B.; Lin, Z.; Ouyang, B.; MacMillan, P.; Ngai, J.; Syed, A.; Sindhwani, S.; Chan, W. Specific Endothelial Cells Govern Nanoparticle Entry into Solid Tumors. *ACS Nano* **2021**, *15* (9), 14080−14094.
(225) Beldman, T.; Malinova, T.; Desclos, E.; Grootemaat, E.; Misiak, A.; van der Velden, S.; van Roomen, C.; Beckers, L.; van Veen, H.; Krawczyk, P.; Hoebe, R.; Sluimer, J.; Neele, A.; de Winther, M.; van der Wel, N.; Lutgens, E.; Mulder, W.; Huveneers, S.; Kluza, E. Nanoparticle-Aided Characterization of Arterial Endothelial Architecture during Atherosclerosis Progression and Metabolic Therapy. *ACS Nano* **2019**, *13* (12), 13759−13774.
(226) Ono, H. *6-well plate for cell culture*. https://togotv.dbcls.jp/en/togopic.2020.213.html (October 14, 2022).
(227) Brinker, C. J. University of New Mexico, Albuquerque, NM. MSNPs in CAM vasculature, 2022. Unpublished Work.
(228) Mar, S.; Xu, J.; Sunnybrook Research Institute, Toronto, ON. Super-resolution Power Doppler Imaging of Tumor Xenografts in the CAM, 2022. Unpublished Work.

https://doi.org/10.1021/acsnano.2c03990
ACS Nano 2022, 16, 19626−19650